



## Article

# Neural Adaptive Funnel Dynamic Surface Control with Disturbance-Observer for the PMSM with Time Delays

Menghan Li <sup>1</sup> , Shaobo Li <sup>2,\*</sup> , Junxing Zhang <sup>2</sup>, Fengbin Wu <sup>3</sup> and Tao Zhang <sup>1</sup>

<sup>1</sup> School of Mechanical Engineering, Guizhou University, Guiyang 550025, China; limenghan1226@163.com (M.L.); zhangtao\_202102@163.com (T.Z.)

<sup>2</sup> State Key Laboratory of Public Big Data, Guizhou University, Guiyang 550025, China; jx\_zhanggz@163.com

<sup>3</sup> School of Computer Science and Technology, Guizhou University, Guiyang 550025, China; wfaceboss@163.com

\* Correspondence: lishaobo@gzu.edu.cn

**Abstract:** This paper suggests an adaptive funnel dynamic surface control method with a disturbance observer for the permanent magnet synchronous motor with time delays. An improved prescribed performance function is integrated with a modified funnel variable at the beginning of the controller design to coordinate the permanent magnet synchronous motor with the output constrained into an unconstrained one, which has a faster convergence rate than ordinary barrier Lyapunov functions. Then, the specific controller is devised by the dynamic surface control technique with first-order filters to the unconstrained system. Therein, a disturbance-observer and the radial basis function neural networks are introduced to estimate unmatched disturbances and multiple unknown nonlinearities, respectively. Several Lyapunov-Krasovskii functionals are constructed to make up for time delays, enhancing control performance. The first-order filters are implemented to overcome the “complexity explosion” caused by general backstepping methods. Additionally, the boundedness and binding ranges of all the signals are ensured through the detailed stability analysis. Ultimately, simulation results and comparison experiments confirm the superiority of the controller designed in this paper.

**Keywords:** disturbance observer; dynamic surface control; permanent magnetic synchronous motor; funnel control; radial basis function neural networks



**Citation:** Li, M.; Li, S.; Zhang, J.; Wu, F.; Zhang, T. Neural Adaptive Funnel Dynamic Surface Control with Disturbance-Observer for the PMSM with Time Delays. *Entropy* **2022**, *24*, 1028. <https://doi.org/10.3390/e24081028>

Academic Editor: Friedhelm Schwenker

Received: 22 June 2022

Accepted: 21 July 2022

Published: 26 July 2022

**Publisher's Note:** MDPI stays neutral with regard to jurisdictional claims in published maps and institutional affiliations.



**Copyright:** © 2022 by the authors. Licensee MDPI, Basel, Switzerland. This article is an open access article distributed under the terms and conditions of the Creative Commons Attribution (CC BY) license (<https://creativecommons.org/licenses/by/4.0/>).

## 1. Introduction

The permanent magnet synchronous motor (PMSM) is a separately excited generator composed of a stator and a rotator. In recent decades, PMSMs are widely used in aerospace, defense, and other major fields due to the advantages of simple structure, small size, and low noise [1,2]. With the purpose of environmental protection, PMSMs are currently also used in the fields of new energy vehicles, and other major fields [3,4]. However, PMSMs are systems with nonlinearities, strong coupling, and time-varying. Hence, there has been considerable interest in the high-precision control of PMSMs, which is of great help to enhance the aviation industry and ecological conservation for a nation.

The most classical method of controlling PMSMs is backstepping control. The backstepping method splits the  $n$ -order complicated system into  $n$  subsystems and realizes the virtual control of every subsystem. In the former  $n - 1$  steps, it will derive a virtual controller in every step, significantly simplifying the computational process of the controller. Nevertheless, the backstepping method also suffers from the “explosion of complexity” caused by the repeated derivatives of the virtual controller, owing to its inherent properties of it. To circumvent this obstacle, a first-order filter combined with the backstepping control approach [5] is created by Swaroop, called dynamic surface control [6]. Despite dynamic surface control methods [7–9], that can reduce computing efforts, various nonlinear factors such as time delays, external disturbances, and physical constraints are ubiquitous in real industrial scenarios [10,11], which may diminish the controlling precision of the PMSM

systems. Researchers have proposed proportional integral derivative (PID) control [12], neural network (NN) [5], time delay control [13,14], disturbance observer (DO) [15,16], and constraint control [17,18] methods for different nonlinearities to reach satisfying control results. Hence, the key point is how to design an effective controller to address the various nonlinear uncertainties such as unknown functions, mismatched disturbance, state constraints, and time delays.

For the unknown characteristics and uncertain disturbances, the NN-based adaptive control that has superb evaluating abilities are employed to obtain the high-performance control of nonlinear systems [19,20]. For instance, the authors in [19] design a radial basis function NN (RBFNN) to estimate the error of the high-gain observer and the lumped interference. The authors in [20] utilize a feedforward artificial NN to renew the training parameters of the proportion integration differential controller, offering high dynamic performance. Due to their advantages, RBFNNs are introduced in this paper to estimate the unknown uncertainties. To achieve advanced transient and steady-state performance, NNs still need to be combined with other control strategies.

For the uncertain load disturbances, considerable pioneering investigations based on the DO have been frequently suggested to achieve the steady operation of the PMSM [21]. Based on the sliding mode control technology, a DO is proposed to attain desired anti-load-disturbance capability [11]. A DO is fused into the super-twisting sliding mode method to compensate for the lumped disturbance [22]. A second-order DO is utilized to estimate the parameters perturbations, ensuring the accuracy of the PMSM system [16]. Though the DO-based schemes can effectively suppress the uncertain perturbations, the transient performance that is significant for the robustness of the system is not negligible. To reduce the calculation burdens and further enhance the transient performance, this paper introduces a finite-time second-order command filter to approximate the matched and mismatched disturbance in a finite time with the aid of these investigations.

The physical constraints complicate controller design process, proper strategies which are proposed by researchers to improve the transient performance and stability of nonlinear systems. They have introduced barrier Lyapunov functions [23], prescribed performance functions (PPF) [24,25], and funnel control strategies. As the novel control methods developed, the barrier Lyapunov functions need to be modified to suit specific changing situations, resulting in its non-universality. Likewise, the demand for precise initial values limits the applications of PPF strategies. Based on these, the improved PPFs are applied to further attain superior transient performance [26,27]. Compared with PPFs and barrier Lyapunov functions, the funnel control method is considered a promising way to deal with the constraints owing to its effectiveness for the output overshoot [28,29], and does not need precise initial conditions. The funnel control method has been applied in vehicles [30], and robots [31] because it can avoid the modification of the controllers. According to the above investigations, this paper suggests a funnel controller for the output-constrained PMSM system to achieve excellent control performance.

It is known that time delays harm the dynamic performance and the stability of the PMSMs. The time delay control strategies that can strengthen both transient and steady-state responses, recently, have been involved in many pioneering backstepping investigations. The studies can be roughly divided into two groups namely Smith predictor control tools [32,33] and Lyapunov-Krasovskii functional methods [34,35]. For example, a smith predictor is combined with the speed controller to eliminate the time delays [32]. An appropriate Lyapunov-Krasovskii functional is employed to ensure the asymptotic stability of the delay-dependent PMSM system [34]. A hyperbolic function is utilized to deal with the delay caused by the low-pass filter [36]. From these, a proper Lyapunov-Krasovskii functional is designed in this paper to address the time delay issues, which enhances both the transient and steady-state performances of PMSM.

Motivated by these discussions, a neural adaptive funnel dynamic surface control (FDSC) scheme combined with the DO is designed in this article to address the output-

restrained system with time delays and load interference. The primary contributions of this paper are outlined as:

- (a) The prescribed performance control method can ensure the tracking error converges to a predefined arbitrary small residual set [24,25]. However, the transient performance still needs to be improved. Upon this, a neural adaptive funnel control strategy with advanced transient performance is proposed to restrict the output response of PMSM into a certain funnel region. The simulation section compares the funnel control method with neural dynamic surface control (NDSC) and PID methods, and the funnel controller has smaller tracking error and better transient performance. The advanced transient performance makes the devised controller more applicable.
- (b) The constraint-considered controller can reasonably simulate the physical constraints in the actual operating environment of the PMSM [23,25]. Nevertheless, there are many other nonlinear factors in the actual industries that need to be taken into account. The FDSC method considers output constraints, time delays, and mismatched external load interference, which allows FDSC to simulate the actual situation more realistically. The Lyapunov-Krasovskii functionals and DO are devised to suppress the time delays and approximate the unmatched external load interference. The simulation section shows that the FDSC method has smaller steady-state and transient errors, and the robustness and dynamic performances are strengthened compared with the NDSC and the PID schemes.

Notation: For any variable  $c, \hat{c}$  denotes the estimated value of  $c, \tilde{c} = c - \hat{c}$  represents the state error.  $\|\bullet\|$  indicates the 2-norm of  $\bullet$ .

## 2. System Formulation and Preliminaries

### 2.1. System Statement

Under the  $(d - q)$  coordinate frame, formulate the PMSM mathematical model as [7]:

$$\begin{cases} \dot{\theta} = \omega \\ \dot{\omega} = 3n_p/(2J)[(L_d - L_q)i_d i_q + \varphi i_q] - B\omega/J - T_L/J \\ \dot{i}_q = -R_s i_q/L_q - n_p L_d \dot{i}_d \omega/L_q - n_p \varphi \omega/L_q + u_q/L_q \\ \dot{i}_d = -R_s i_d/L_d + n_p L_q i_q \omega/L_d + u_d/L_d \end{cases} \quad (1)$$

where  $u_q$  and  $u_d$  are control variables. The descriptions of PMSM parameters are exhibited in Table 1.

**Table 1.** Parameters of PMSM.

Parameters	Descriptions	Units
$\theta$	Rotor angular	rad
$\omega$	Rotor angular velocity, $\dot{\theta}$	rad/s
$\dot{\omega}$	First-order derivative of rotor angular velocity	rad/s <sup>2</sup>
$i_d, i_q$	Currents of $d - q$ axis	A
$u_d, u_q$	Voltages of $d - q$ axis	V
$L_d, L_q$	Stator inductances of $d - q$ axis	H
$J$	Inertia rotor moment	kg·m <sup>2</sup>
$B$	Friction coefficient	N·m/(rad/s)
$\varphi$	Inertia magnet flux linkage	Wb
$R_s$	Armature resistance	$\Omega$
$n_p$	Pole pairs	
$T_L$	Load torque	N·m

To simplify (1), define  $a_1 = 3n_p\varphi/2, a_2 = 3n_p(L_d - L_q)/2, b_1 = -R_s/L_q, b_2 = -n_p L_d/L_q, b_3 = -n_p\varphi/L_q, b_4 = 1/L_q, c_1 = -R_s/L_d, c_2 = n_p L_q/L_d, c_3 = 1/L_d$ .

Moreover, describe the states variables as:

$$x_1 = \theta, x_2 = \omega, x_3 = i_q, x_4 = i_d. \tag{2}$$

Considering time delays and asymmetric output constraints, the model (1) can be reconstructed as:

$$\begin{cases} \dot{x}_1 = x_2 + \Delta l_1[x(t - \tau_1)] \\ \dot{x}_2 = \frac{a_1}{J}x_3 + \frac{a_2}{J}x_3x_4 - \frac{B}{J}x_2 - \frac{T_L}{J} + \Delta l_2[x(t - \tau_2)] + \Delta E \\ \dot{x}_3 = b_1x_3 + b_2x_2x_4 + b_3x_2 + b_4u_q + \Delta l_3[x(t - \tau_3)] \\ \dot{x}_4 = c_1x_4 + c_2x_2x_3 + c_3u_d + \Delta l_4[x(t - \tau_4)], \end{cases} \tag{3}$$

where  $x = (x_1, x_2, x_3, x_4)^T \in R^4$ , and the state variable  $x_1$  subjects to:

$$x_1 \in \Pi_{x_1} := \{x_1 \in R : x_d(t) - f_1(t) < x_1(t) < x_d(t) + f_1(t)\}. \tag{4}$$

**Remark 1.** In the actual PMSM operating environment, there are plenty of unknown uncertainties, such as time delays, physical constraints, and matched and mismatched disturbances. It is essential to consider these limitations in the PMSM system to guarantee that the controller designed in this paper approach reality. It is worth mentioning that for the PMSM systems, the unmatched interference  $\Delta E$  and the time delays  $\Delta l_i(x(t - \tau_i)), i = 1, \dots, 4$  in (3) as well as the time-varying symmetric output constraints in (4) are firstly considered simultaneously. Thereby, the controller devised here based on (3) is more suitable for real industrial fields.

Based on the above observations, the control objective of this paper is to devise a neural adaptive funnel dynamic surface controller based on DO for (3) to realize:

- (a) The system output  $x_1$  tracks the desired signal  $x_d$ , where the transient control behavior of (3) can be retained by (4).
- (b) The other signals in the resulting system are bounded.

To ensure these objectives, the following assumption and lemmas are provided.

**Assumption 1 ([37]).** The continuous desired signal  $x_d(t)$  and its  $i$ th-order derivatives  $x_d^{(i)}(t)$ , ( $i = 0, \dots, 4$ ) are bounded. The continuous state-constrained functions  $f_1(t)$  as well as its  $j$ th-order derivatives  $f_1^{(j)}(t)$ , ( $j = 0, \dots, 4$ ) are bounded.

**Lemma 1 ([38]).** For any  $f(\eta_1, \dots, \eta_n) : R^{m_1} \times \dots \times R^{m_n} \rightarrow R$ , there are smooth functions  $\omega_i(\eta_i) > 0 : R^{m_i} \rightarrow R$  satisfying  $|f(\eta_1, \dots, \eta_n)| \leq \sum_{i=1}^n \omega_i(\eta_i)$ . For the initial value  $f(0, \dots, 0) = 0, \omega_i(0) = 0$  fulfills  $|f(0, \dots, 0)| \leq \sum_{i=1}^n \omega_i(0)$  as well.

**Remark 2.** According to Lemma 1, there are continuous positive functions  $\xi_{ik}, i = 1, \dots, 4$  restricting the time-delay terms  $\Delta l_i(x(t - \tau_i)), i = 1, \dots, 4$  in the system (3) as  $\Delta l_i(x(t - \tau_i)) \leq \sum_{k=1}^4 \xi_{ik}(x_k(t - \tau_i))$ . With the aid of Young's inequality, it leads to:

$$e_i \Delta l_i[x(t - \tau_i)] \leq 1/2ne_i^2 + 1/2 \sum_{j=1}^n \xi_{ij}^2(x_j(t - \tau_i)), i = 1, \dots, 4. \tag{5}$$

**Lemma 2 ([39,40]).** For any real variables  $p, q$ , and the positive constants  $m_i, i = 1, 2, 3$ , the following inequality holds:

$$|a|^{m_1}|b|^{m_2} \leq \frac{m_1}{m_1 + m_2} m_3 |a|^{m_1+m_2} + \frac{m_2}{m_1 + m_2} m_3^{-m_1/m_2} |b|^{m_1+m_2}. \tag{6}$$

**Lemma 3 ([41]).** For  $\sigma > 0$ , there exists the set  $\Omega_e := \{e \in R : |e| \leq 0.2554\sigma\}$ . For  $e \notin \Omega_e$ , the inequality  $1 - 16 \tanh^2(e/\sigma) < 0$  holds.

Thereafter, function arguments are sometimes dropped without confusion.

### 2.2. Neural Network Systems and Function Approximation

Since the RBFNNs can approximate the unknown hard-to-calculated functions that are in a closed set at any precision [42,43], this paper introduces an RBFNN function to estimate unknown functions  $W(X)$ :

$$W(X) = \varphi^{*T}P(X) + \psi(X), \quad \forall X \in \Omega_X, \tag{7}$$

where  $X = [x_1, x_2, \dots, x_n]^T$  indicates the input vector,  $\psi(X)$  fulfills  $|\psi(X)| < \psi_M$  with a bounded constant  $\psi_M$ .  $P(X) = [p_1(x), p_2(x), \dots, p_l(x)]^T$  is a vector of basis function, and select  $p_i(x)$  as the versatile Gaussian functions:

$$p_i(x) = \exp\left[-(x - v_i)^T(x - v_i)/\chi_i^2\right], \quad i = 1, 2, \dots, m. \tag{8}$$

Construct the expected weight vector  $\varphi^*$  as:

$$\varphi^* = \arg \min_{\varphi \in R^n} \left\{ \sup_{X \in D_X} \|W(X) - \hat{\varphi}^T P(X)\| \right\}. \tag{9}$$

The 2-norms of the variables are utilized to assess the weights allowing for a reduction in the computational burden of RBFNN [42,43]. Consequently, it leads to:

$$\beta_i = \|\varphi_i\|^2 = \varphi_i^T \varphi_i, \quad i = 1, \dots, 4. \tag{10}$$

### 3. Design of Neural Adaptive Funnel Control

This section introduces the funnel controller designed in this paper. In Section 3.1, a funnel-type variable with improved PPF is introduced to remove the output constraint of the variable  $x_1$ . In Section 3.2, a DO is proposed to approximate the matched and mismatched disturbance that is utilized in step 2. In Section 3.3, four steps are listed to show the whole design procedure of the funnel controller for the PMSM system.

#### 3.1. Funnel Control with Improved Prescribed Performance Function

The core point of the funnel control is devising the given functions of the envelope as the boundaries that restrict the tracking error  $s_1(t)$ , where  $s_1(t) = x_1 - x_d$ . Based on this idea, a funnel-type function is selected at the very beginning of the controller design as:

$$g(t) = F_k(f_1(t), G(t), \|s_1(t)\|). \tag{11}$$

A PPF  $f^*(t)$  [44] is constructed to obtain both steady-state and transient performances of  $s_1(t)$ :

$$f^*(t) = (f_0 - f_\infty) \exp(-\pi t) + f_\infty, \tag{12}$$

where the design parameters  $3 f_0 > f_\infty > 0$  and the minimum convergence rate value  $\pi > 0$ .

From [44], we can attain that the control objectives can be achieved when the following condition satisfied:

$$|s_1(t)| < \omega f^*(t), \tag{13}$$

where the design constants  $\omega > 0$ .

To obtain better steady performance, a funnel control with envelope boundaries is introduced. An improved PPF based on (12) is proposed:

$$f_1(t) = f_0 \exp(-\pi t) + \frac{t}{\pi(t+1)} f_\infty, \tag{14}$$

where  $f_\infty / \pi$  represents the steady-state error.

**Remark 3.** The improved PPF  $f_1(t)$  indicated by (14) has the same properties as (12). Moreover, the improved PPF has a faster convergence speed and more outstanding transient performance than the conventional PPF while choosing the same parameters values of  $f_0, f_\infty, \pi$ . As an example, Figure 1 gives the profiles of (14) and (12) with  $f_0 = 1, f_\infty = 0.05, \pi = 3, 5, 10$ .

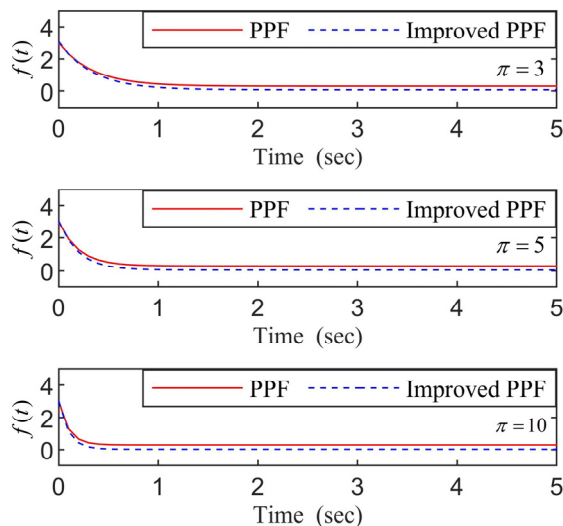


Figure 1. The curves of PPF and improved PPF ( $\pi = 3, 5, 10$ ).

The gain function  $F_k(\cdot)$  [31] can be regulated by:

$$F_k(f_1(t), G(t), \|s_1(t)\|) = G(t) / (f_1(t) - \|s_1(t)\|). \tag{15}$$

It can be concluded from (15) that the value of  $F_k(\cdot)$  decreases as  $f_1(t)$  moves away from  $\|s_1(t)\|$  when  $G(t)$  is supposed to be fixed. Regrettably, the gain  $F_k(\cdot)$  formulated by (15) is not differentiable at the point of  $s_1(t) = 0$ , which does not meet the using conditions of backstepping.

To circumvent the obstacle, a modified funnel variable  $\eta_1$  by virtue of (14) and [31] is first created as follows:

$$\eta_1 = s_1^2 / (f_1^2 - s_1^2). \tag{16}$$

**Remark 4.** If  $f_1 \rightarrow s_1$ , the value of  $\eta_1$  will be infinite. For this reason, assuming that the starting value of the tracking error  $s_1(0)$  is limited by the funnel boundaries. Choosing a proper design parameter  $f_0$  can effectively eliminate the infinite starting value.

**Remark 5.** Compared with prescribed performance control [45], the improved PPF-based funnel control not only provides better transient performance but is also simpler and more efficient without calculating inverse conversion errors, which is conducive to the stable operation of PMSM.

The time derivatives of  $\eta_i$  in (16) are obtained as:

$$\dot{\eta}_1 = \frac{2s_1 f_1^2}{(f_1^2 - s_1^2)^2} \left( \dot{s}_1 - s_1 \frac{\dot{f}_1}{f_1} \right) = \Gamma_1 \left( \dot{s}_1 - s_1 \frac{\dot{f}_1}{f_1} \right), \tag{17}$$

where the variable  $\Gamma_1 = 2s_1 f_1^2 / (f_1^2 - s_1^2)^2$ .



### 3.2. Disturbance Observer

For the difficult-to-compute external disturbance, a DO is an effective utensil to observe the matched and mismatched interference. Hence, introduce the intermediate variables  $d, D$ , and conceive the DO as [46]:

$$\begin{cases} \dot{\hat{x}}_2 = a_1/Jx_3 + a_2/Jx_3x_4 - B/Jx_2 - T_L/J + \Delta l_2(x(t - \tau_2)) + \Delta E_1 \\ \Delta E_1 = -\kappa_1 t_1^{1/3} |\hat{x}_2 - x_2|^{2/3} \text{sgn}(\hat{x}_2 - x_2) + \Delta \hat{E}_2 \\ \Delta \dot{\hat{E}}_2 = -\kappa_1 t_1^{1/2} |\Delta \hat{E}_2 - \Delta E_2|^{1/2} \text{sgn}^{1/2}(\Delta \hat{E}_2 - \Delta E_2) + \Delta \dot{\hat{E}} \\ \Delta \dot{\hat{E}} = -\kappa_2 t_1 \text{sgn}(\Delta \hat{E} - \Delta \dot{\hat{E}}_2), \end{cases} \quad (18)$$

where coefficients  $\kappa_1 > 0, \kappa_2 > 0, t_1 > 0$ .

Describing variables as  $\tilde{x}_2 = \hat{x}_2 - x_2, \Delta \tilde{E} = \Delta \hat{E} - \Delta E, \Delta \tilde{E}_2 = \Delta \hat{E}_2 - \Delta E_2$ , it leads to:

$$\begin{cases} \dot{\tilde{x}}_2 = -\kappa_1 t_1^{1/3} |\tilde{x}_2 - x_2|^{2/3} \text{sgn}(\tilde{x}_2 - x_2) + \Delta \tilde{E} \\ \Delta \dot{\tilde{E}} = -\kappa_1 t_1^{1/2} |\Delta \hat{E}_2 - \Delta E_2|^{1/2} \text{sgn}(\Delta \hat{E}_2 - \Delta E_2) + (\Delta \hat{E} - \Delta E) \\ \Delta \dot{\tilde{E}} \in -\kappa_2 t_1 \text{sgn}(\Delta \hat{E} - \Delta \dot{\hat{E}}_2) + [-t_1, t_1]. \end{cases} \quad (19)$$

Supposing a negligible rate of change for load disturbance  $\Delta E_2$ , then it is bounded. According to  $\Delta \tilde{E}_2 = \Delta \hat{E}_2 - \Delta E_2$ , it can be concluded that  $\Delta \tilde{E}$  is bounded. Similarly, we can attain that  $\Delta \hat{E}$  and  $\hat{x}_2$  are limited to the small adjacency of  $\Delta E$  and  $x_2$ , respectively.

**Remark 6.** The interference error can be well estimated by the excellent DO (18). In other words, we can select suitable parameters  $\kappa_1, \kappa_2$  and  $t_1$  to tackle the matched and unmatched load disturbance. Moreover, the excellent DO can prevent the system tremors due to the symbolic function in the classical sliding mode control method simultaneously [21].

### 3.3. Neural Adaptive Funnell Controller Design

This subsection will provide a dynamic surface controller by integrating the funnel control technology. First of all, let us introduce the following coordinate conversion:

$$e_1 = \eta_1, e_2 = x_2 - u_{2c}, e_3 = x_3 - u_{3c}, e_4 = x_4. \quad (20)$$

Define the first-order filters as:

$$\lambda_i \dot{u}_{ic} + u_{ic} = u_i, u_{ic}(0) = u_i(0), i = 2, 3, \quad (21)$$

where  $\lambda_i$  are constants.

**Remark 7.** This paper introduces first-order filters to bypass the repeated derivatives of  $u_i$  so that the “explosion of complexity” can be eliminated by designing proper filters. However, there exist filter errors that influence the control precision by introducing the first-order filters into the controller design procedure. When choosing proper Lyapunov functions to devise the virtual and actual controller, the filter errors need to be taken into account to improve the control accuracy.

Akin to (20), describe the filter errors  $\phi_i$  as:

$$\phi_i = u_{ic} - u_i, i = 2, 3. \quad (22)$$

Fusing (3) and (16) into (20), and take the derivatives of  $e_i, i = 1, \dots, 4$  in (20):





Taking the derivative of  $V_T$  in (26) obtains:

$$\dot{V}_T = \frac{1}{2} \sum_{i=1}^4 \sum_{j=1}^4 \exp[-\lambda(t - \tau_i)] \zeta_{ij}^2[x_j(t)] - \frac{1}{2} \sum_{i=1}^4 \sum_{j=1}^4 \zeta_{ij}^2[x_j(t - \tau_i)] - \lambda V_T. \tag{27}$$

With (24) and (27), deriving  $V_1$  in (25) yields:

$$\dot{V}_1 = e_1 \dot{e}_1 - \frac{1}{d_1} \tilde{\beta}_1 \dot{\beta}_1 + \frac{1}{2} \sum_{i=1}^4 \sum_{j=1}^4 \exp[-\lambda(t - \tau_i)] \zeta_{ij}^2[x_j(t)] - \frac{1}{2} \sum_{i=1}^4 \sum_{j=1}^4 \zeta_{ij}^2[x_j(t - \tau_i)] + \phi_2 \dot{\phi}_2 - \lambda V_T. \tag{28}$$

Fusing (23) into (28) generates:

$$\begin{aligned} \dot{V}_1 = e_1 \Gamma_1 \left\{ e_2 + \phi_2 + u_2 - \dot{x}_d + \Delta l_1[x(t - \tau_1)] - s_1 \frac{\dot{f}_1}{f_1} \right\} - \frac{1}{2} \sum_{i=1}^4 \sum_{j=1}^4 \zeta_{ij}^2[x_j(t - \tau_i)] \\ + \frac{1}{2} \sum_{i=1}^4 \sum_{j=1}^4 \exp[-\lambda(t - \tau_i)] \zeta_{ij}^2[x_j(t)] - \frac{1}{d_1} \tilde{\beta}_1 \dot{\beta}_1 - \lambda V_T + \phi_2 \dot{\phi}_2. \end{aligned} \tag{29}$$

Based on Remark 2 with  $n = 4$ , the following inequality can be obtained:

$$e_1 \Gamma_1 \Delta l_1[x(t - \tau_1)] \leq 2e_1^2 \Gamma_1^2 + \frac{1}{2} \sum_{j=1}^4 \zeta_{1j}^2[x_j(t - \tau_1)]. \tag{30}$$

Taking (30) into (29) derives:

$$\dot{V}_1 \leq e_1 \Gamma_1 \left( e_2 + \phi_2 + u_2 - \dot{x}_d - s_1 \frac{\dot{f}_1}{f_1} \right) - \frac{1}{2} \sum_{i=2}^4 \sum_{j=1}^4 \zeta_{ij}^2[x_j(t - \tau_i)] - \frac{1}{d_1} \tilde{\beta}_1 \dot{\beta}_1 + 2e_1^2 \Gamma_1^2 + T(x) + \phi_2 \dot{\phi}_2 - \lambda V_T, \tag{31}$$

where the time delay function  $T(x) = 1/2 \sum_{i=1}^4 \sum_{j=1}^4 (-\exp(\lambda \tau_i) \zeta_{ij}^2(x_j(t)))$ . We can infer that  $\lim_{e_1 \rightarrow 0} (T(x)/e_1) \rightarrow \infty$ . Consequently,  $(16/e_1) \tanh^2(e_1/\sigma_1) T$  is brought in (32) to further eliminate the time delays. Then, rewrite (31) as:

$$\begin{aligned} \dot{V}_1 \leq e_1 \left[ \Gamma_1 e_2 + \Gamma_1 \phi_2 + \Gamma_1 u_2 + \frac{16}{e_1} T \tanh^2\left(\frac{e_1}{\sigma_1}\right) + 2e_1 \Gamma_1^2 - \Gamma_1 \dot{x}_d - \Gamma_1 s_1 \frac{\dot{f}_1}{f_1} \right] \\ + \phi_2 \dot{\phi}_2 - \lambda V_T + \left[ 1 - 16 \tanh^2\left(\frac{e_1}{\sigma_1}\right) \right] T - \frac{1}{2} \sum_{i=2}^4 \sum_{j=1}^4 \zeta_{ij}^2[x_j(t - \tau_i)] - \frac{1}{d_1} \tilde{\beta}_1 \dot{\beta}_1. \end{aligned} \tag{32}$$

Then this paper utilizes an unknown function  $W_1(X_1)$  to generalize the unknown functions:

$$W_1(X_1) = 3e_1 \Gamma_1^2 + e_1 + 16/e_1 T \tanh^2(e_1/\sigma_1) - \Gamma_1 \dot{x}_d, \tag{33}$$

where  $W_1(X_1)$  is an unknown function. According to (11), (16) and (20), it can be learned that  $e_1$  is composed of a known desired signal  $x_d$  and an unknown state  $x_1$ ,  $\Gamma_1$  consists of a known desired signal  $x_d$ , an assured function  $f_1$ , and an unknown state  $x_1$ . The RBFNN is developed to estimate the unknown function  $W_1(X_1)$ , then  $X_1 = [x_1, \dots, x_4, x_d, \dot{x}_d]^T$ .

For the unknown and uncertain functions, RBFNN is considered as a promising tool to approximate them at any precision. An RBFNN is designed to approximate  $W_1(X_1)$ :

$$W_1(X_1) = \varphi_1^T P_1(X_1) + \psi_1(X_1), \quad |\psi_1(X_1)| \leq \psi_M, \tag{34}$$

where  $\psi_M$  stands for the positive bounded constant.

As it can be seen from (33), (32) can be simplified by an RBFNN:

$$\begin{aligned} \dot{V}_1 \leq & e_1 \left( \Gamma_1 e_2 + \Gamma_1 \phi_2 + \Gamma_1 u_2 + \varphi_1^T P_1(X_1) + \psi_1(X_1) - \Gamma_1 s_1 \frac{\dot{f}_1}{f_1} - e_1 \Gamma_1^2 - e_1 \right) - \frac{1}{d_1} \tilde{\beta}_1 \dot{\hat{\beta}}_1 \\ & + \left[ 1 - 16/e_1 T \tanh^2(e_1/\sigma_1) \right] T + \phi_2 \dot{\phi}_2 - \lambda V_T - \frac{1}{2} \sum_{i=2}^4 \sum_{j=1}^4 \xi_{ij}^2 [x_j(t - \tau_i)]. \end{aligned} \tag{35}$$

According to (34) and Lemma 2 with  $m_1 = m_2 = m_3 = 1$ , functions that are difficult to compute can be deflated to:

$$\begin{cases} e_1 \Gamma_1 \phi_2 \leq e_1^2 \Gamma_1^2 + \frac{1}{4} \phi_2^2 \\ e_1 W_1(X_1) = e_1 [\varphi_1^T P_1(X_1) + \psi_1(X_1)] \leq \frac{1}{4\mu_1^2} \beta_1 e_1^2 P_1^T P_1 + \mu_1^2 + \frac{\psi_M^2}{4} + e_1^2, \end{cases} \tag{36}$$

where  $\mu_1$  stands for the positive design constant.

Integrating (36) into (35) generates:

$$\begin{aligned} \dot{V}_1 \leq & e_1 \left( \Gamma_1 e_2 + \Gamma_1 u_2 - \Gamma_1 s_1 \frac{\dot{f}_1}{f_1} \right) + \left[ 1 - 16 \tanh^2\left(\frac{e_1}{\sigma_1}\right) \right] T - \frac{1}{2} \sum_{i=2}^4 \sum_{j=1}^4 \xi_{ij}^2 [x_j(t - \tau_i)] - \frac{1}{d_1} \tilde{\beta}_1 \dot{\hat{\beta}}_1 \\ & - \lambda V_T + \phi_2 \dot{\phi}_2 + \frac{1}{4\mu_1^2} e_1^2 \beta_1 P_1^T P_1 + \frac{1}{4} \phi_2^2 + \frac{\psi_M^2}{4} + \mu_1^2. \end{aligned} \tag{37}$$

Devise the stunning control law  $u_2$  and the adaptive law  $\dot{\hat{\beta}}_1$  as:

$$\begin{aligned} u_2 &= -\frac{(f_1^2 - s_1^2) s_1}{2f_1^2} \left( k_1 + \frac{1}{4\mu_1^2} \hat{\beta}_1 P_1^T P_1 \right) + s_1 \frac{\dot{f}_1}{f_1} \\ \dot{\hat{\beta}}_1 &= \frac{d_1}{4\mu_1^2} e_1^2 P_1^T P_1 - \gamma_1 \hat{\beta}_1, \end{aligned} \tag{38}$$

where the design constants  $k_1 > 0, \gamma_1 > 0$ .

Inserting the control law  $u_2$  and adaptive law  $\dot{\hat{\beta}}_1$  in (38) into (37) derives:

$$\begin{aligned} \dot{V}_1 \leq & -k_1 e_1^2 + \left[ 1 - 16 \tanh^2\left(\frac{e_1}{\sigma_1}\right) \right] T - \frac{1}{2} \sum_{i=2}^4 \sum_{j=1}^4 \xi_{ij}^2 [x_j(t - \tau_i)] + \frac{\gamma_1}{d_1} \tilde{\beta}_1 \hat{\beta}_1 \\ & - \lambda V_T + \Gamma_1 e_1 e_2 + \phi_2 \dot{\phi}_2 + \mu_1^2 + \frac{\psi_M^2}{4} + \frac{\phi_2^2}{4}. \end{aligned} \tag{39}$$

According to (21)–(24), and (38), differentiate the filter error  $\phi_2$  in (22) as:

$$\dot{\phi}_2 = \dot{u}_{2c} - \dot{u}_2 = -\frac{\dot{\phi}_2}{\lambda_2} + M_2(e_1, e_2, \phi_2, \hat{\beta}_1, x_d, \dot{x}_d, \ddot{x}_d), \tag{40}$$

where  $M_2(e_1, e_2, \phi_2, \hat{\beta}_1, x_d, \dot{x}_d, \ddot{x}_d)$  is a smooth function.

In virtual of [47], we can infer that there exists an upper value  $\overline{M}_2 (\overline{M}_2 \geq 0)$  for the original conditions to restrict  $M_2(e_1, e_2, \phi_2, \hat{\beta}_1, x_d, \dot{x}_d, \ddot{x}_d)$  within the prescribed set, it produces:

$$\dot{\phi}_2 \leq -\frac{\phi_2}{\lambda_2} + \overline{M}_2, \tag{41}$$

where  $\overline{M}_2 > |M_2(e_1, e_2, \phi_2, \hat{\beta}_1, x_d, \dot{x}_d, \ddot{x}_d)|$ .

Based on Lemma 2 with  $m_1 = m_2 = m_3 = 1$ , consider  $a = \phi_2, b = \overline{M}_2$ . Then, the hard-to-compute function is converted into:

$$\phi_2 \dot{\phi}_2 = -\phi_2^2 / \lambda_2 + \phi_2 \overline{M}_2 \leq -(1/\lambda_2 - 1/4) \phi_2^2 + \overline{M}_2^2. \tag{42}$$

Substituting (42) into (39) generates:

$$\begin{aligned} \dot{V}_1 \leq & -k_1 e_1^2 - 1/2 \sum_{i=2}^4 \sum_{j=1}^4 \zeta_{ij}^2 [x_j(t - \tau_i)] - \left(\frac{1}{\lambda_2} - \frac{1}{4}\right) \phi_2^2 + \left[1 - 16 \tanh^2\left(\frac{e_1}{\sigma_1}\right)\right] T + \frac{\gamma_1}{d_1} \tilde{\beta}_1 \hat{\beta}_1 \\ & - \lambda V_T + \Gamma_1 e_1 e_2 + \bar{M}_2^2 + \psi_M^2/4 + \mu_1^2. \end{aligned} \tag{43}$$

**Step 2.** The design of the stunning control law  $u_3$  and the adaptive law  $\hat{\beta}_2$ .

Considering the state error  $e_2$ , filter error  $\phi_3$  and the approximation error  $\tilde{\beta}_2$ , the second Lyapunov function  $V_2$  is chosen as:

$$V_2 = V_1 + 1/2 e_2^2 + 1/2 \phi_3^2 + 1/(2d_2) \tilde{\beta}_2^2, \tag{44}$$

where  $d_2$  denotes the positive constants.

With (24), taking the derivative of  $V_2$  in (44) leads to:

$$\dot{V}_2 = \dot{V}_1 + e_2 \dot{e}_2 + \phi_3 \dot{\phi}_3 - 1/d_2 \tilde{\beta}_2 \dot{\hat{\beta}}_2. \tag{45}$$

Integrating (23) and (43) into (45) produces:

$$\begin{aligned} \dot{V}_2 \leq & -k_1 e_1^2 - 1/2 \sum_{i=2}^4 \sum_{j=1}^4 \zeta_{ij}^2 [x_j(t - \tau_i)] - \left(\frac{1}{\lambda_2} - \frac{1}{4}\right) \phi_2^2 + \left[1 - 16 \tanh^2\left(\frac{e_1}{\sigma_1}\right)\right] T + \frac{\gamma_1}{d_1} \tilde{\beta}_1 \hat{\beta}_1 \\ & + e_2 \{e_3 + \phi_3 + u_3 + (a_1/J - 1)x_3 + a_2/J x_3 x_4 - B/J x_2 - T_L/J + \Delta l_2 [x(t - \tau_2)] \\ & - \dot{u}_{2c} + \Delta E\} - \lambda V_T + \phi_3 \dot{\phi}_3 + \Gamma_1 e_1 e_2 + \bar{M}_2^2 + \mu_1^2 + \psi_M^2/4 - 1/d_2 \tilde{\beta}_2 \dot{\hat{\beta}}_2. \end{aligned} \tag{46}$$

Resembling (30), define  $n = 4$ , then it derives:

$$e_2 \Delta l_2 [x(t - \tau_2)] \leq 2e_2^2 + \frac{1}{2} \sum_{j=1}^4 \zeta_{2j}^2 [x_j(t - \tau_2)]. \tag{47}$$

Assume that  $|\Delta \hat{E} - \Delta E = \Delta \tilde{E}| \leq q_1$ , and the constant  $q_1 > 0$ . It is hard to determine the positive and negative of  $e_2$ , an inequality  $(\Delta \hat{E} - \Delta E)e_2 \leq |\Delta \hat{E} - \Delta E||e_2| \leq q_1|e_2|$  is brought to ensure that the following inequality holds. Pouring (47) into (46) gets:

$$\begin{aligned} \dot{V}_2 \leq & -k_1 e_1^2 - \frac{1}{2} \sum_{i=3}^4 \sum_{j=1}^4 \zeta_{ij}^2 [x_j(t - \tau_i)] - \left(\frac{1}{\lambda_2} - \frac{1}{4}\right) \phi_2^2 + \left[1 - 16 \tanh^2\left(\frac{e_1}{\sigma_1}\right)\right] T + \frac{\gamma_1}{d_1} \tilde{\beta}_1 \hat{\beta}_1 \\ & + e_2 [e_3 + \phi_3 + \Delta \hat{E} + (a_1/J - 1)x_3 + u_3 - B/J x_2 + a_2/J x_3 x_4 - T_L/J + 2e_2 - \dot{u}_{2c} \\ & + \Gamma_1 e_1] - \lambda V_T + \phi_3 \dot{\phi}_3 + \bar{M}_2^2 + q_1 |e_2| + \mu_1^2 + \psi_M^2/4 - 1/d_2 \tilde{\beta}_2 \dot{\hat{\beta}}_2. \end{aligned} \tag{48}$$

Design  $F_2(X_2)$  as

$$F_2(X_2) = \left(\frac{a_1}{J} - 1\right) x_3 + \frac{a_2}{J} x_3 x_4 - \frac{B}{J} x_2 - \frac{T_L}{J} + 4e_2 + \Gamma_1 e_1, \tag{49}$$

where  $e_1 = x_1 - x_d, e_2 = x_2 - a_{2c}, \Gamma_1$  is composed of a known desired signal  $x_d$ , a given function  $f_1$ , and an unknown state  $x_1$ . Based on the structure of the uncertain function  $F_2(X_2)$ ,  $X_2$  is composed of  $x_1, x_2, x_3, x_4, x_d$  and  $u_{2c}$ . Then it leads to  $X_2 = [x_1, \dots, x_4, x_d, u_{2c}]^T$ .

A piecewise function  $W_2(X_2)$  is devised as:

$$W_2(X_2) = \begin{cases} F_2(X_2) - q_1, & e_2 \leq 0 \\ F_2(X_2) + q_1, & e_2 > 0, \end{cases} \tag{50}$$

where  $X_2 = [x_1, \dots, x_4, x_d, u_{2c}]^T$ .

Integrating (50) into (48) generates:

$$\begin{aligned} \dot{V}_2 \leq & -k_1 e_1^2 - \frac{1}{2} \sum_{i=2}^4 \sum_{j=1}^4 \tilde{\zeta}_{ij}^2 [x_j(t - \tau_i)] - \left(\frac{1}{\lambda_2} - \frac{1}{2}\right) \phi_2^2 - \frac{1}{d_2} \tilde{\beta}_2 \dot{\beta}_2 + \left[1 - 16 \tanh^2\left(\frac{e_1}{\sigma_1}\right)\right] T + \frac{\gamma_1}{d_1} \tilde{\beta}_1 \hat{\beta}_1 \\ & + e_2 [e_3 + \phi_3 + u_3 + \Delta \hat{E} + W_2(X_2) - 2e_2 - \dot{u}_{2c}] - \lambda V_T + \phi_3 \dot{\phi}_3 + \overline{M}_2^2 + \mu_1^2 + \frac{\psi_M^2}{4}. \end{aligned} \tag{51}$$

Akin to (34), the unknown function  $W_2(X_2)$  can be approximated by an RBFNN:

$$W_2(X_2) = \wp_2^T P_2(X_2) + \psi_2(X_2), \quad |\psi_2(X_2)| < \psi_M. \tag{52}$$

Re-express (51) as:

$$\begin{aligned} \dot{V}_2 \leq & -k_1 e_1^2 - \frac{1}{2} \sum_{i=3}^4 \sum_{j=1}^4 \tilde{\zeta}_{ij}^2 [x_j(t - \tau_i)] - \left(\frac{1}{\lambda_2} - \frac{1}{2}\right) \phi_2^2 + \left[1 - 16 \tanh^2\left(\frac{e_1}{\sigma_1}\right)\right] T + \frac{\gamma_1}{d_1} \tilde{\beta}_1 \hat{\beta}_1 \\ & + e_2 [e_3 + \phi_3 + u_3 + \Delta \hat{E} + \wp_2^T P_2(X_2) + \psi_2(X_2) - \dot{u}_{2c} - 2e_2] - \lambda V_T + \phi_3 \dot{\phi}_3 + \overline{M}_2^2 \\ & + \mu_1^2 + \psi_M^2/4 - 1/d_2 \tilde{\beta}_2 \dot{\beta}_2. \end{aligned} \tag{53}$$

Similar to (36), the inequalities below can be obtained with  $m_1 = m_2 = m_3 = 1$ :

$$\begin{cases} e_2 \phi_3 \leq e_2^2 + \frac{1}{4} \phi_3^2 \\ e_2 W_2(X_2) = e_2 [\wp_2^T P_2(X_2) + \psi_2(X_2)] \leq 1/(4\mu_2^2) \beta_2 e_2^2 P_2^T P_2 + \mu_2^2 + \psi_M^2/4 + e_2^2, \end{cases} \tag{54}$$

where  $\mu_2$  represents the positive design parameter.

Integrating (54) into (53) produces:

$$\begin{aligned} \dot{V}_2 \leq & -k_1 e_1^2 - \frac{1}{2} \sum_{i=3}^4 \sum_{j=1}^4 \tilde{\zeta}_{ij}^2 [x_j(t - \tau_i)] - \left(\frac{1}{\lambda_2} - \frac{1}{2}\right) \phi_2^2 + \left[1 - 16 \tanh^2\left(\frac{e_1}{\sigma_1}\right)\right] T + \frac{\gamma_1}{d_1} \tilde{\beta}_1 \hat{\beta}_1 \\ & + e_2 (e_3 + u_3 + \Delta \hat{E} - \dot{u}_{2c}) - \lambda V_T + \phi_3 \dot{\phi}_3 + \overline{M}_2^2 + \sum_{i=1}^2 \mu_i^2 + \frac{\psi_M^2}{2} + \frac{\phi_3^2}{4} \\ & + \frac{1}{4\mu_2^2} e_2^2 \beta_2 P_2^T P_2 - \frac{1}{d_2} \tilde{\beta}_2 \dot{\beta}_2. \end{aligned} \tag{55}$$

Analogous to (38), choose the stunning control law  $u_3$  and the adaptive law  $\dot{\hat{\beta}}_2$  as:

$$\begin{aligned} u_3 &= -\left(k_2 e_2 + \frac{1}{4\mu_2^2} \hat{\beta}_2 e_2 P_2^T P_2 + \Delta \hat{E}\right) + \dot{u}_{2c} \\ \dot{\hat{\beta}}_2 &= \frac{d_2}{4\mu_2^2} e_2^2 P_2^T P_2 - \gamma_2 \hat{\beta}_2, \end{aligned} \tag{56}$$

where the design parameters  $k_2 > 0, \gamma_2 > 0$ .

**Remark 9.** Up to this step, the external interference  $\Delta E$  can be thoroughly approximated by the DO (18) with the stunning controller (56), thus the stable operation of the controlled system is further enhanced.

Pouring stunning control law  $u_3$  and the adaptive law  $\dot{\hat{\beta}}_2$  in (56) into (55) leads to:

$$\begin{aligned} \dot{V}_2 \leq & -\sum_{i=1}^2 k_i e_i^2 - \frac{1}{2} \sum_{i=3}^4 \sum_{j=1}^4 \tilde{\zeta}_{ij}^2 [x_j(t - \tau_i)] - \left(\frac{1}{\lambda_2} - \frac{1}{2}\right) \phi_2^2 + \sum_{i=1}^2 \frac{\gamma_i}{d_i} \tilde{\beta}_i \hat{\beta}_i + \left[1 - 16 \tanh^2\left(\frac{e_1}{\sigma_1}\right)\right] T \\ & - \lambda V_T + e_2 e_3 + \phi_3 \dot{\phi}_3 + \overline{M}_2^2 + \sum_{i=1}^2 \mu_i^2 + \psi_M^2/2 + \phi_3^2/4. \end{aligned} \tag{57}$$

Akin to (42), we can obtain:

$$\phi_3 \dot{\phi}_3 \leq -\left(\frac{1}{\lambda_3} - \frac{1}{4}\right) \phi_3^2 + \overline{M}_3^2, \tag{58}$$

where the function  $\overline{M}_3 > 0$ .

Substituting (58) into (57) produces:

$$\begin{aligned} \dot{V}_2 \leq & -\sum_{i=1}^2 k_i e_i^2 - \frac{1}{2} \sum_{i=3}^4 \sum_{j=1}^4 \zeta_{ij}^2 [x_j(t - \tau_i)] - \sum_{i=2}^3 \left( \frac{1}{\lambda_i} - \frac{1}{2} \right) \phi_i^2 + \sum_{i=1}^2 \frac{\gamma_i}{d_i} \tilde{\beta}_i \hat{\beta}_i + \left[ 1 - 16 \tanh^2 \left( \frac{e_1}{\sigma_1} \right) \right] T \\ & - \lambda V_T + e_2 e_3 + \sum_{i=1}^2 \mu_i^2 + \sum_{i=2}^3 \bar{M}_i^2 + \psi_M^2 / 2. \end{aligned} \tag{59}$$

**Step 3.** The design of the actual controller  $u_q$  and the adaptive law  $\dot{\hat{\beta}}_3$ .

With the state error  $e_3$  and estimation error  $\tilde{\beta}_3$  considered, the third Lyapunov function  $V_3$  is chosen as:

$$V_3 = V_2 + \frac{1}{2} e_3^2 + \frac{1}{2d_3} \tilde{\beta}_3^2, \tag{60}$$

where  $d_3$  stands for the known positive constant.

Based on (24), derive  $V_3$  in (60) as:

$$\dot{V}_3 = \dot{V}_2 + e_3 \dot{e}_3 - \frac{1}{d_3} \tilde{\beta}_3 \dot{\hat{\beta}}_3. \tag{61}$$

Combining (23) and (59), (61) becomes:

$$\begin{aligned} \dot{V}_3 \leq & -\sum_{i=1}^2 k_i e_i^2 - \frac{1}{2} \sum_{i=3}^4 \sum_{j=1}^4 \zeta_{ij}^2 [x_j(t - \tau_i)] - \sum_{i=2}^3 \left( \frac{1}{\lambda_i} - \frac{1}{2} \right) \phi_i^2 + \sum_{i=1}^2 \frac{\gamma_i}{d_i} \tilde{\beta}_i \hat{\beta}_i + \left[ 1 - 16 \tanh^2 \left( \frac{e_1}{\sigma_1} \right) \right] T + \frac{\psi_M^2}{2} \\ & - \lambda V_T + e_3 \{ b_1 x_3 + b_3 x_2 + b_2 x_2 x_4 + b_4 u_q + \Delta l_3 [x(t - \tau_3)] + e_2 - \dot{u}_{3c} \} + \sum_{i=1}^2 \mu_i^2 + \sum_{i=2}^3 \bar{M}_i^2 - \frac{1}{d_3} \tilde{\beta}_3 \dot{\hat{\beta}}_3. \end{aligned} \tag{62}$$

Analogous to (30), the following inequality holds with  $n = 4$ :

$$e_3 \Delta l_3 [x(t - \tau_3)] \leq 2e_3^2 + \frac{1}{2} \sum_{j=1}^4 \zeta_{3j}^2 [x_j(t - \tau_3)]. \tag{63}$$

Pouring (63) into (62) leads to:

$$\begin{aligned} \dot{V}_3 \leq & -\sum_{i=1}^2 k_i e_i^2 - \frac{1}{2} \sum_{j=1}^4 \zeta_{ij}^2 [x_j(t - \tau_i)] - \sum_{i=2}^3 \left( \frac{1}{\lambda_i} - \frac{1}{2} \right) \phi_i^2 + \sum_{i=1}^2 \frac{\gamma_i}{d_i} \tilde{\beta}_i \hat{\beta}_i + \left[ 1 - 16 \tanh^2 \left( \frac{e_1}{\sigma_1} \right) \right] T + \frac{\psi_M^2}{2} \\ & - \lambda V_T + e_3 (b_1 x_3 + b_3 x_2 + b_2 x_2 x_4 + b_4 u_q + e_2 + 2e_3 - \dot{u}_{3c}) + \sum_{i=1}^2 \mu_i^2 + \sum_{i=2}^3 \bar{M}_i^2 - \frac{1}{d_3} \tilde{\beta}_3 \dot{\hat{\beta}}_3. \end{aligned} \tag{64}$$

Design the unknown function  $W_3(X_3)$  as:

$$W_3(X_3) = b_1 x_3 + b_2 x_2 x_4 + b_3 x_2 + e_2 + 3e_3, \tag{65}$$

where  $e_2 = x_2 - \alpha_{2c}$ ,  $e_3 = x_3 - \alpha_{3c}$ . According to the composition of the unknown function  $W_3(X_3)$ , it can be derived that  $X_3$  consists of the unknown and uncertain states  $x_2, x_3, x_4, \alpha_{2c}$  and  $\alpha_{3c}$ . Then  $X_3 = [x_2, x_3, x_4, u_{2c}, u_{3c}]^T$ .

Consequently, rewrite (64) as:

$$\begin{aligned} \dot{V}_3 \leq & -\sum_{i=1}^2 k_i e_i^2 - \frac{1}{2} \sum_{j=1}^4 \zeta_{ij}^2 [x_j(t - \tau_i)] - \sum_{i=2}^3 \left( \frac{1}{\lambda_i} - \frac{1}{2} \right) \phi_i^2 + \sum_{i=1}^2 \frac{\gamma_i}{d_i} \tilde{\beta}_i \hat{\beta}_i + \left[ 1 - 16 \tanh^2 \left( \frac{e_1}{\sigma_1} \right) \right] T \\ & - \lambda V_T + e_3 [W_3(X_3) + b_4 u_q - e_3 - \dot{u}_{3c}] + \sum_{i=1}^2 \mu_i^2 + \sum_{i=2}^3 \bar{M}_i^2 + \psi_M^2 / 2 - 1/d_3 \tilde{\beta}_3 \dot{\hat{\beta}}_3. \end{aligned} \tag{66}$$

Utilize an RBFNN to approximate  $W_3(X_3)$ :

$$W_3(X_3) = \wp_3^T P_3(X_3) + \psi_3(X_3), \quad |\psi_3(X_3)| \leq \psi_M. \tag{67}$$

Resembling (36), it generates:

$$e_3 W_3(X_3) = e_3 \left[ \varphi_3^T P_3(X_3) + \psi_3(X_3) \right] \leq \frac{1}{4\mu_3^2} \beta_3 e_3^2 P_3^T P_3 + \mu_3^2 + \frac{\psi_M^2}{4} + e_3^2, \tag{68}$$

where  $\mu_3$  represents the positive design parameter.  
Then, reperform (66) as:

$$\begin{aligned} \dot{V}_3 \leq & -\sum_{i=1}^2 k_i e_i^2 - \frac{1}{2} \sum_{j=1}^4 \zeta_{ij}^2 [x_j(t - \tau_i)] - \sum_{i=2}^3 \left( \frac{1}{\lambda_i} - \frac{1}{2} \right) \phi_i^2 + \sum_{i=1}^2 \frac{\gamma_i}{d_i} \tilde{\beta}_i \hat{\beta}_i + \left[ 1 - 16 \tanh^2 \left( \frac{e_1}{\sigma_1} \right) \right] T + \frac{3}{4} \psi_M^2 \\ & - \lambda V_T + e_3 (b_4 u_q - \dot{u}_{3c}) + \sum_{i=2}^3 \bar{M}_i^2 + \sum_{i=1}^3 \mu_i^2 + \frac{1}{4\mu_3^2} e_3^2 \beta_3 P_3^T P_3 - \frac{1}{d_3} \tilde{\beta}_3 \dot{\hat{\beta}}_3. \end{aligned} \tag{69}$$

Design the real controller  $u_q$  and the adaptive law  $\dot{\hat{\beta}}_3$  as:

$$\begin{aligned} u_q &= -\frac{1}{b_4} \left( k_3 e_3 + \frac{1}{4\mu_3^2} \hat{\beta}_3 e_3 P_3^T P_3 - \dot{u}_{3c} \right) \\ \dot{\hat{\beta}}_3 &= \frac{d_3}{4\mu_3^2} e_3^2 P_3^T P_3 - \gamma_3 \hat{\beta}_3, \end{aligned} \tag{70}$$

where the design parameters  $k_3 > 0, \gamma_3 > 0$ .

At this point, the actual controller for the  $q$ -axis has been designed.

Inserting the real controller  $u_q$  and the adaptive law  $\dot{\hat{\beta}}_3$  in (70) into (69) derives:

$$\begin{aligned} \dot{V}_3 \leq & -\sum_{i=1}^3 k_i e_i^2 - \frac{1}{2} \sum_{j=1}^4 \zeta_{ij}^2 [x_j(t - \tau_i)] - \sum_{i=2}^3 \left( \frac{1}{\lambda_i} - \frac{1}{2} \right) \phi_i^2 + \sum_{i=1}^3 \frac{\gamma_i}{d_i} \tilde{\beta}_i \hat{\beta}_i + \left[ 1 - 16 \tanh^2 \left( \frac{e_1}{\sigma_1} \right) \right] T \\ & - \lambda V_T + \sum_{i=2}^3 \bar{M}_i^2 + \sum_{i=1}^3 \mu_i^2 + \frac{3}{4} \psi_M^2. \end{aligned} \tag{71}$$

**Step 4.** The design of the actual controller  $u_d$  and the adaptive law  $\dot{\hat{\beta}}_4$ .

Consider the state error  $e_4$  and the estimation error  $\tilde{\beta}_4$ , then the Lyapunov function  $V_4$  is chosen as:

$$V_4 = V_3 + 1/2e_4^2 + 1/(2d_4)\tilde{\beta}_4^2, \tag{72}$$

where  $d_4$  represents the positive design parameter.

Combining (24), differentiate  $V_4$  in (72) produces:

$$\dot{V}_4 = \dot{V}_3 + e_4 \dot{e}_4 - 1/d_4 \tilde{\beta}_4 \dot{\hat{\beta}}_4. \tag{73}$$

Integrating (23) and (71) into (73) yields:

$$\begin{aligned} \dot{V}_4 \leq & -\sum_{i=1}^3 k_i e_i^2 - \frac{1}{2} \sum_{j=1}^4 \zeta_{ij}^2 [x_j(t - \tau_i)] - \sum_{i=2}^3 \left( \frac{1}{\lambda_i} - \frac{1}{2} \right) \phi_i^2 + \sum_{i=1}^3 \frac{\gamma_i}{d_i} \tilde{\beta}_i \hat{\beta}_i + \left[ 1 - 16 \tanh^2 \left( \frac{e_1}{\sigma_1} \right) \right] T \\ & - \lambda V_T + e_4 \{ c_1 x_4 + c_2 x_2 x_3 + \Delta l_4 [x(t - \tau_4)] + c_3 u_d \} + 3/4 \psi_M^2 + \sum_{i=2}^3 \bar{M}_i^2 + \sum_{i=1}^3 \mu_i^2 \\ & - \frac{1}{d_4} \tilde{\beta}_4 \dot{\hat{\beta}}_4. \end{aligned} \tag{74}$$

Analogous to (30), the following inequality holds with  $n = 4$ :

$$e_4 \Delta l_4 [x(t - \tau_4)] \leq 2e_4^2 + \frac{1}{2} \sum_{j=1}^4 \zeta_{4j}^2 [x_j(t - \tau_4)]. \tag{75}$$

Design the unknown function  $W_4(X_4)$  as:

$$W_4(X_4) = c_1 x_4 + c_2 x_2 x_3 + 3e_4, \tag{76}$$



where  $e_4 = x_4$ , the uncertain function  $X_4$  consists of  $x_2, x_3$  and  $x_4$ . Then  $X_4 = [x_2, x_3, x_4]^T$ . Then, (74) can be redrafted as:

$$\begin{aligned} \dot{V}_4 \leq & -\sum_{i=1}^3 k_i e_i^2 - \sum_{i=2}^3 \left(\frac{1}{\lambda_i} - \frac{1}{2}\right) \phi_i^2 + \sum_{i=1}^3 \frac{\gamma_i}{d_i} \tilde{\beta}_i \hat{\beta}_i + \left[1 - 16 \tanh^2\left(\frac{e_1}{\sigma_1}\right)\right] T + \sum_{i=2}^3 \bar{M}_i^2 + \sum_{i=3}^3 \mu_i^2 \\ & - \lambda V_T + e_4 [W_4(X_4) + c_3 u_d - e_4] + 3/4 \psi_M^2 - 1/d_4 \tilde{\beta}_4 \dot{\hat{\beta}}_4. \end{aligned} \tag{77}$$

Similarly, the unknown function  $W_4(X_4)$  can be estimated by an RBFNN:

$$W_4(X_4) = \varphi_4^T P_4(X_4) + \psi_4(X_4), \quad |\psi_4(X_4)| \leq \psi_M. \tag{78}$$

Pouring (78) into (77) leads to:

$$\begin{aligned} \dot{V}_4 \leq & -\sum_{i=1}^3 k_i e_i^2 - \sum_{i=2}^3 \left(\frac{1}{\lambda_i} - \frac{1}{2}\right) \phi_i^2 - \frac{1}{d_4} \tilde{\beta}_4 \dot{\hat{\beta}}_4 + \sum_{i=2}^3 \bar{M}_i^2 + \sum_{i=1}^3 \frac{\gamma_i}{d_i} \tilde{\beta}_i \hat{\beta}_i + \left[1 - 16 \tanh^2\left(\frac{e_1}{\sigma_1}\right)\right] T \\ & - \lambda V_T + e_4 [-e_4 + c_3 u_d + \varphi_4^T P_4(X_4) + \psi_4(X_4)] + \sum_{i=1}^3 \mu_i^2 + 3/4 \psi_M^2. \end{aligned} \tag{79}$$

Analogous to (36), it derives:

$$e_4 W_4(X_4) = e_4 [\varphi_4^T P_4(X_4) + \psi_4(X_4)] \leq \frac{1}{4\mu_4^2} e_4^2 \beta_4 P_4^T P_4 + \mu_4^2 + \frac{\psi_M^2}{4} + e_4^2, \tag{80}$$

where  $\mu_4$  stands for the positive design parameter.

Combining (80) with (79) generates:

$$\begin{aligned} \dot{V}_4 \leq & -\sum_{i=1}^3 k_i e_i^2 - \sum_{i=2}^3 \left(\frac{1}{\lambda_i} - \frac{1}{2}\right) \phi_i^2 - \frac{1}{d_4} \tilde{\beta}_4 \dot{\hat{\beta}}_4 + \sum_{i=2}^3 \bar{M}_i^2 + \sum_{i=1}^3 \frac{\gamma_i}{d_i} \tilde{\beta}_i \hat{\beta}_i + \left[1 - 16 \tanh^2\left(\frac{e_1}{\sigma_1}\right)\right] T \\ & - \lambda V_T + c_3 e_4 u_d + \sum_{i=1}^4 \mu_i^2 + \psi_M^2 + \frac{1}{4\mu_4^2} e_4^2 \beta_4 P_4^T P_4. \end{aligned} \tag{81}$$

Devise the real controller  $u_d$  and the adaptive law  $\dot{\hat{\beta}}_4$  as:

$$\begin{aligned} u_d &= -\frac{1}{c_3} [k_4 e_4 + 1/(4\mu_4^2) \hat{\beta}_4 e_4 P_4^T P_4] \\ \dot{\hat{\beta}}_4 &= \frac{d_4}{4\mu_4^2} e_4^2 P_4^T P_4 - \gamma_4 \hat{\beta}_4, \end{aligned} \tag{82}$$

where the design constants  $k_4 > 0, \gamma_4 > 0$ .

Fusing the real controller  $u_d$  and the adaptive law  $\dot{\hat{\beta}}_4$  in (82) into (81) produces:

$$\begin{aligned} \dot{V} \leq & -\sum_{i=1}^4 k_i e_i^2 - \sum_{i=2}^3 (1/\lambda_i - 1/2) \phi_i^2 + \sum_{i=2}^3 \bar{M}_i^2 + \sum_{i=1}^4 \gamma_i / d_i \tilde{\beta}_i \hat{\beta}_i \\ & - \lambda V_T + \sum_{i=1}^4 \mu_i^2 + \psi_M^2 + \left[1 - 16 \tanh^2(e_1/\sigma_1)\right] T. \end{aligned} \tag{83}$$

At the very beginning of this subsection, a funnel variable (16) based on modified PPF is designed in this paper to guarantee that the tracking error narrows down to a prescribed funnel type scope. The modified PPF avoids the demand for the precise initial value of the output variable. Among these steps, RBFNNs are utilized to approximate the unknown hard-to-compute functions (33), (50), (65) and (76) based on their infinite approximation capability. The Lyapunov Krasovskii functional eliminates the time delays  $\Delta l_i[x(t - \tau_i)]$  in (3) with the aid of Lemma 1 and Remark 2. A DO (18) is introduced in step 2 to observe the uncertain matched and mismatched disturbance.

Up to this step, the design process of the FDSC with time delays and output constraints is finished. The effectiveness of the controller and the boundedness of all the variables need to be discussed in Section 4 and proved in Section 5.

#### 4. Stability Analysis

For arbitrary predefined  $p > 0$ , the compact sets are described as:

$$\left\{ \begin{aligned} \Omega_1 &= \left\{ (e_1, \phi_2, \hat{\beta}_1, \zeta_{11}, \zeta_{12}, \dots, \zeta_{44}) : 2 e_1^2 + 2\phi_2^2 + \frac{2}{d_1} \tilde{\beta}_1^2 + 4V_T \leq 4p \right\} \\ \Omega_2 &= \left\{ \left( \begin{array}{c} e_1, e_2, \phi_2, \phi_3, \hat{\beta}_1, \hat{\beta}_2, \\ \zeta_{11}, \zeta_{12}, \dots, \zeta_{44} \end{array} \right) : 2 \sum_{i=1}^2 e_i^2 + 2 \sum_{i=2}^3 \phi_i^2 + \sum_{i=1}^2 \frac{2}{d_i} \tilde{\beta}_i^2 + 4V_T \leq 4p \right\} \\ \Omega_3 &= \left\{ \left( \begin{array}{c} e_1, e_2, e_3, \phi_2, \phi_3, \hat{\beta}_1, \hat{\beta}_2, \\ \hat{\beta}_3, \zeta_{11}, \zeta_{12}, \dots, \zeta_{44} \end{array} \right) : 2 \sum_{i=1}^3 e_i^2 + 2 \sum_{i=2}^3 \phi_i^2 + \sum_{i=1}^3 \frac{2}{d_i} \tilde{\beta}_i^2 + 4V_T \leq 4p \right\} \\ \Omega_4 &= \left\{ \left( \begin{array}{c} e_1, \dots, e_4, \phi_2, \phi_3, \hat{\beta}_1, \dots, \\ \hat{\beta}_4, \zeta_{11}, \zeta_{12}, \dots, \zeta_{44} \end{array} \right) : 2 \sum_{i=1}^4 e_i^2 + 2 \sum_{i=2}^3 \phi_i^2 + \sum_{i=1}^4 \frac{2}{d_i} \tilde{\beta}_i^2 + 4V_T \leq 4p \right\}. \end{aligned} \right. \tag{84}$$

**Theorem 1.** According to Assumption 1, the neural adaptive FDSC approach designed for the PMSM system (3) in this paper includes four controllers  $u_2, u_3, u_q, u_d$  and four adaptive laws  $\dot{\hat{\beta}}_i, i = 1, \dots, 4$ . For the initial conditions, if  $\Omega_i, i = 1, \dots, 4, -f_1(0) < s_1(0) < f_1(0)$  and  $x_d \in (-d, d)$  are fulfilled, the core purposes of this paper will be realized.

**Proof of Theorem 1.** This part proves the boundedness and the binding ranges of the variables, demonstrating the effectiveness of the designed controller in this paper for the PMSM system. □

4.1. Verification of the Boundedness for All Variables

Considering the state errors  $e_i, i = 1, \dots, 4$ , the filter errors  $\phi_i, i = 1, 2$ , and the estimation errors  $\tilde{\beta}_i, i = 1, \dots, 4$ , design the whole Lyapunov function  $V$  as:

$$V = V_4 = 1/2 \sum_{i=1}^4 e_i^2 + 1/2 \sum_{i=2}^3 \phi_i^2 + \sum_{i=1}^4 1/(2d_i) \tilde{\beta}_i^2. \tag{85}$$

Then, it can be taken from (83) the derivative of  $V$  in (85) as:

$$\begin{aligned} \dot{V} \leq & -\sum_{i=1}^4 k_i e_i^2 - \sum_{i=2}^3 (1/\lambda_i - 1/2) \phi_i^2 + \sum_{i=2}^3 \bar{M}_i^2 + \sum_{i=1}^4 \gamma_i / d_i \tilde{\beta}_i \hat{\beta}_i \\ & - \tilde{\lambda} V_T + \sum_{i=1}^4 \mu_i^2 + \psi_M^2 + [1 - 16 \tanh^2(e_1/\sigma_1)] T. \end{aligned} \tag{86}$$

Reorganize (86) as:

$$\dot{V} \leq -b_0 V + \varphi_0 + a_1, \tag{87}$$

where  $b_0 = \min\{2k_1, 2k_2, 2k_3, 2k_4, 2\gamma_1, 2\gamma_2, 2\gamma_3, 2\gamma_4, \tilde{\lambda}, (2/\lambda_2 - 1), (2/\lambda_3 - 1)\}$ ,  $\varphi_0 = \sum_{i=1}^4 \mu_i^2 + \sum_{i=2}^3 \bar{M}_i^2 + \psi_M^2, a_1 = [1 - 16 \tanh^2(e_1/\sigma_1)] T$ .

To ensure every term in (87) satisfying the stability conditions, it needs to choose proper design parameters that make up  $b_0$  to guarantee  $b_0 > 0$ . With the aid of Lemma 3, the value of  $a_1$  in (87) depends on two cases: (I) For  $e_1 \notin \Omega_{e_1}$ , we can deduce that  $a_1 \leq 0$  due to  $T(x) \geq 0$ ; (II) For  $e_1 \in \Omega$ , it can be inferred that  $|e_1| \leq 0.2554\sigma_1$  and  $\sigma_1 > 0$ . Based on the above discussion, we can conclude that the boundedness of  $e_1$  and  $a_1$  are both assured. Consequently, a constant  $\varphi_1 > 0$  can be chosen to fulfill  $|\varphi_0 + a_1| < \varphi_1$ . Then redraft (87) as:

$$\dot{V} \leq -b_0 V + \varphi_1. \tag{88}$$

Multiplying both sides by  $\exp(b_0 t)$ , then (88) becomes  $d(V(t) \exp(b_0 t))/dt \leq \varphi_1 \exp(b_0 t)$ . Integrating the inequality over  $[0, t]$ , it leads to:

$$V(t) \leq \left[ V(0) - \frac{\varphi_1}{b_0} \right] \exp(b_0 t) + \frac{\varphi_1}{b_0} \leq V(0) + \frac{\varphi_1}{b_0}. \tag{89}$$

Especially, the following results can be derived from (89):

$$\lim_{t \rightarrow \infty} |e_i| \leq \sqrt{\frac{2\varphi_1}{b_0}}, i = 1, \dots, 4. \tag{90}$$

It can be derived that  $e_i, i = 1, \dots, 4$  are bounded. Analogously, the boundedness of  $\varphi_2, \varphi_3$ , and  $\tilde{\beta}_i, i = 1, \dots, 4$  are ensured with (85). From (24), it can be concluded that  $\hat{\beta}_i, i = 1, \dots, 4$  are bounded. We can know that  $s_1$  is bounded from (16). Furthermore, it can be obtained that  $x_1$  is bounded according to  $s_1 = x_1 - x_d$  and the boundedness of  $x_d$ . Then, the virtual controller  $u_2$  is bounded based on (38). Consequently, the boundedness of  $x_2$  can be ensured from (20) and (21). Similarly, it can be derived that  $u_2, u_d, u_q, x_i, i = 2, 3, 4$  are also bounded. As a result, the designed controller demonstrates that all the signals of the closed-loop are uniformly bounded.

#### 4.2. Deduction of the Binding Ranges for Variables

According to (85), one derives:

$$e_i^2 \leq 2 \left[ V(0) - \frac{\varphi_1}{b_0} \right] e^{-b_0 t} + \frac{2\varphi_1}{b_0}, i = 2, 3, 4. \tag{91}$$

Then we can get that  $|e_i| \leq \sqrt{2[V(0) - \varphi_1/b_0] \exp(-b_0 t) + 2\varphi_1/b_0}$ .  $|e_i| \leq \sqrt{2\varphi_1/b_0}$  when  $V(0) = \varphi_1/b_0$ . If  $V(0) \neq \varphi_1/b_0$ , for arbitrary known  $\sqrt{2[V(0) - \varphi_1/b_0] \exp(-b_0 t) + 2\varphi_1/b_0} > 2\sqrt{\varphi_1/b_0}$ , there exists  $T$  for each  $t > T$ , it produces  $\sqrt{2[V(0) - \varphi_1/b_0] \exp(-b_0 t) + 2\varphi_1/b_0}$ . When  $t \rightarrow \infty$ , the transformation error  $|e_i| \leq \sqrt{2\varphi_1/b_0}$ .

According to (16),  $\eta_1 \rightarrow \pm\infty$  when and only when  $s_1 \rightarrow \pm f_1$ , it means that if  $e_1 \rightarrow \pm f_1$ ,  $\Delta f_i$  will approach infinite. For the arbitrary starting value  $\Delta f_i$ , it satisfies  $|s_1(0)| < f_1(0)$ . For arbitrary  $t > 0$ , it derives  $|s_1(t)| < f_1(t)$ . According to  $s_1 = x_1 - x_d$ , we can obtain the arbitrary initial condition  $x_d(0) - f_1(0) < x_1(0) < x_d(0) + f_1(0)$  and other conditions  $x_1 \in \Pi_{x_1} := \{x_1 \in R : y_d(t) - f_1(t) < x_1(t) < y_d(t) + f_1(t)\}$  with  $t > 0$ .

**Remark 10.** The quality of the FDSC is judged by the value of  $e_1$ . Hence, it is of great importance to choose parameters based on the selection principle. The value of  $e_1$  depends on  $\varphi_1$  and  $b_0$ . When  $\varphi_1$  decreases and  $b_0$  increases,  $e_1$  will approach zero. Furthermore, we can increase  $\psi_M, \Gamma_1, \sum_{i=1}^4 \mu_i, \sum_{i=2}^3 \bar{M}_i$  and decrease  $\tilde{\lambda}, \varepsilon_2, 1/\lambda_2, 1/\lambda_3, k_i, \gamma_i, i = 1, \dots, 4$  in (87) to achieve excellent control performance of the system.

### 5. Simulation and Comparison Results

#### 5.1. Design of Controllers

To verify the effectiveness of the FDSC method, this subsection provides (3) with two simulation cases: (I) The case 1 contains time delays; (II) The case 2 ignores time delays ( $\Delta f_i = 0, i = 1, 2, 3, 4$ ). PID and NDSC approaches are used as comparison substrates in each case to more visually illustrate the superiority of the FDSC solution.

Select the inherent PMSM parameters as:  $J = 0.003798 \text{Kg}\cdot\text{m}^2, B = 0.001158 \text{N}\cdot\text{m}/(\text{rad}/\text{s}), T_L = 1.5, \varphi = 0.1245 \text{Wb}, L_d = 0.00285 \text{H}, n_p = 3, L_q = 0.00315 \text{H}, R_s = 0.68 \Omega$ . The desired signal and the disturbance function are chosen as  $x_d = 0.02 \sin(2t) + 0.1$  and  $\Delta E = 40x_2 \sin(2t)$ , respectively.

##### 5.1.1. FDSC

Based on Remark 10 and trial and error, the detailed FDSC's design parameters as selected and shown in Table 2 to ensure the tracking error  $e_1$  small enough:

**Table 2.** FDSC’s design parameters.

Parameters	Values	Parameters	Values	Parameters	Values
$u_{2c}(0)$	0	$\hat{\beta}_1(0)$	−0.05	$d_1$	0.65
$u_{3c}(0)$	0.5	$\hat{\beta}_2(0)$	0	$d_2$	0.95
$\varepsilon_2$	0.1	$\hat{\beta}_3(0)$	−0.5	$d_3$	0.75
$\varepsilon_3$	0.01	$\hat{\beta}_4(0)$	0	$d_4$	35
$k_1$	10	$\gamma_1$	60	$\mu_1$	0.06
$k_2$	20	$\gamma_2$	4	$\mu_2$	0.3
$k_3$	20	$\gamma_3$	60	$\mu_3$	0.1
$k_4$	1200	$\gamma_4$	0.4	$\mu_4$	0.01

5.1.2. NDSC

By virtual of [48], select the following variables of NDSC:

$$\begin{cases} e_1 = x_1 - x_d & e_2 = x_3 - \vartheta_{3c} & e_2 = x_2 - \vartheta_{2c} & e_4 = x_4 \\ \dot{u}_{2c} = 1/\varepsilon_2(e_2 - e_{2c}) & \dot{u}_{3c} = 1/\varepsilon_3(u_3 - u_{3c}) & & \\ u_2 = -k_1e_1 + \dot{x}_d & u_3 = J/a_1(-k_2\ell_2 + \dot{u}_{2c} - \hat{\beta}_2^T P_2(X_2)) & & \\ u_q = 1/b_4(-k_3e_3 + \dot{\vartheta}_{3c} - \hat{\beta}_3^T P_3(X_3)) & u_d = J/c_3(-k_4e_4 - \hat{\beta}_4^T P_4(X_4)) & & \\ \dot{\hat{\beta}}_2 = \chi_2[P_2(X_2)e_2 - \gamma_2\hat{\beta}_2] & \dot{\hat{\beta}}_3 = \chi_3[P_3(X_3)e_3 - \gamma_3\hat{\beta}_3] & & \\ \dot{\hat{\beta}}_4 = \chi_4[P_4(X_4)e_4 - \gamma_4\hat{\beta}_4], & & & \end{cases} \quad (92)$$

based on Remark 10 and trial and error, the design parameters are chosen to guarantee the tracking error small enough:  $k_1 = 30, k_2 = k_3 = k_4 = 80, \chi_2 = \chi_3 = \chi_4 = 10, \gamma_2 = \gamma_3 = \gamma_4 = 0.09, \lambda_2 = \lambda_3 = 0.01$ .

5.1.3. PID

According to [12], the following PID controller was chosen with  $u_d = 0$ :

$$u_q = k_p s_1 + k_i \int_0^t s_1 d\tau + k_d d(s_1)/dt, \quad (93)$$

based on Remark 10 and trial and error, the design parameters are chosen to guarantee the tracking error small enough:  $k_p = 20, k_i = 0.05, k_d = 1.5$ .

Meanwhile, Table 3 lists three quantitative indicators to compare FDSC scheme with the NDSC and PID methods.

- (a) Integration over the absolute value of the error (IAE):

$$J_{IAE} = \int_0^t |\ell(\tau)| d\tau. \quad (94)$$

- (b) Integration over time and the absolute value of the error (ITAE):

$$J_{ITAE} = \int_0^t \tau |\ell(\tau)| d\tau. \quad (95)$$

- (c) Integration over squared error (ISE):

$$J_{ISE} = \int_0^t \ell^2(\tau) d\tau. \quad (96)$$

**Table 3.** Comparative numerical results of performance indicators.

Indicators		FDSC	PID	NDSC
Case 1	ISE	0.000661	0.079390	0.244500
	ITAE	0.005941	8.171000	2.801000
	IAE	0.012980	1.091000	0.978600
Case 2	ISE	0.000661	0.079010	0.247000
	ITAE	0.005894	8.151000	2.764000
	IAE	0.012980	1.089000	0.970700

Upon the above discussions, consider the two cases as:

**Case 1:** Select the time-delay terms as:

$$\begin{cases} \Delta f_1(x(t - \tau_1)) = 10x_1^4(t - \tau_1)x_2(t - \tau_1)x_3(t - \tau_1)x_4(t - \tau_1) \\ \Delta f_2(x(t - \tau_2)) = 12x_1^4(t - \tau_2)x_2^4(t - \tau_2)x_3(t - \tau_2)x_4(t - \tau_2) \\ \Delta f_3(x(t - \tau_3)) = 14x_1^4(t - \tau_3)x_2^4(t - \tau_3)x_3^4(t - \tau_3)x_4(t - \tau_3) \\ \Delta f_4(x(t - \tau_4)) = 16x_1^4(t - \tau_4)x_2^4(t - \tau_4)x_3^4(t - \tau_4)x_4^4(t - \tau_4). \end{cases} \quad (97)$$

Design the time-varying funnel type boundaries as  $f_1(t) = e^{-2t} + 0.1t/(2t + 2)$ , and select the original values of the state variables as  $x_i(0) = 0.01, i = 1, \dots, 4$ . Each RBFNN consists of 11 nodes with the center positioned in the interval  $[-11, 11]$ , and the width is 10.

**Case 2:** The time-delay terms are  $\Delta f_i = 0, i = 1, 2, 3, 4$ . In other words, the time-delays are not considered.

5.2. Simulation Comparison Results

The simulation comparison results are shown in Figures 3–7, every figure contains two sub-figures: Case 1 and Case 2. The simulation results will prove the superiority of the FDSC scheme, and justify whether the Lyapunov-Krasovskii functional is effective.

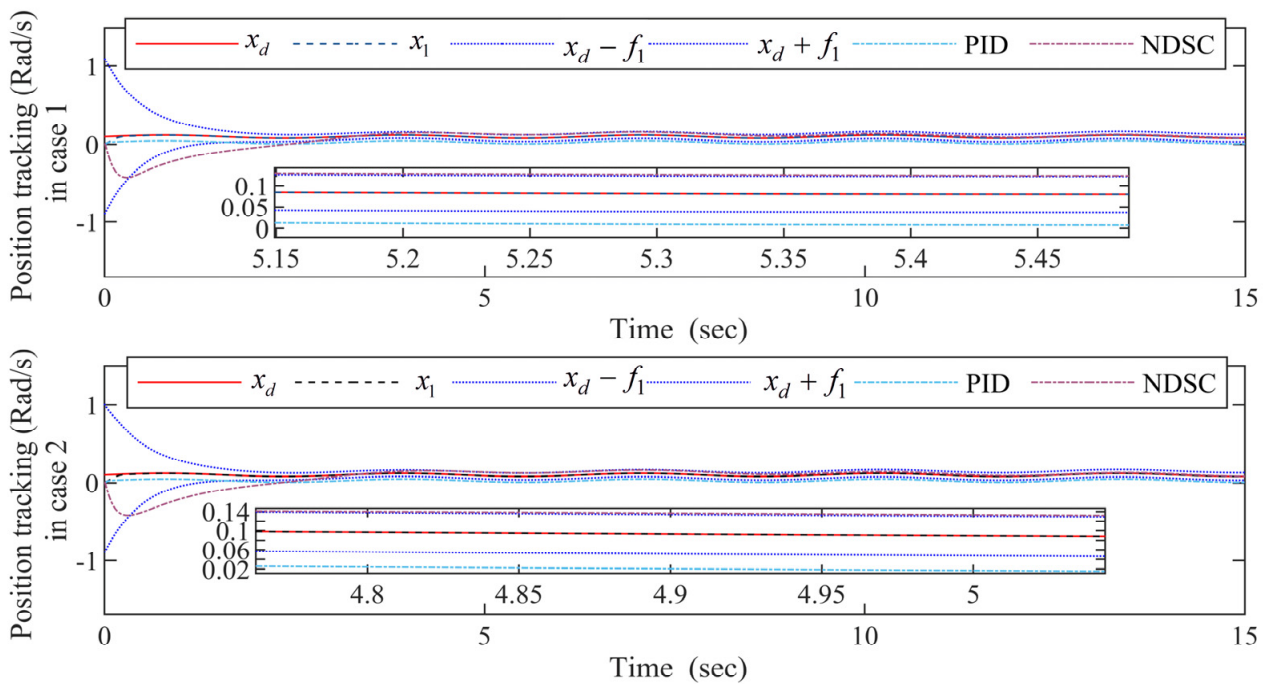


**Figure 3.** The output signal  $x_1$  and the ideal signal  $x_d$  curves for the FDSC, PID, and NDSC.

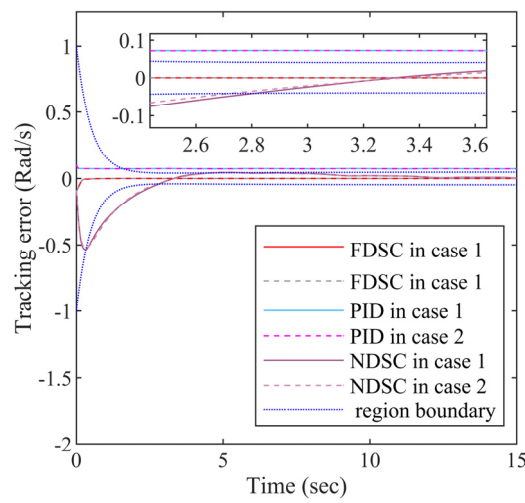


Figure 4. The tracking error responses  $s_1$  for the FDSC, PID, and NDSC.

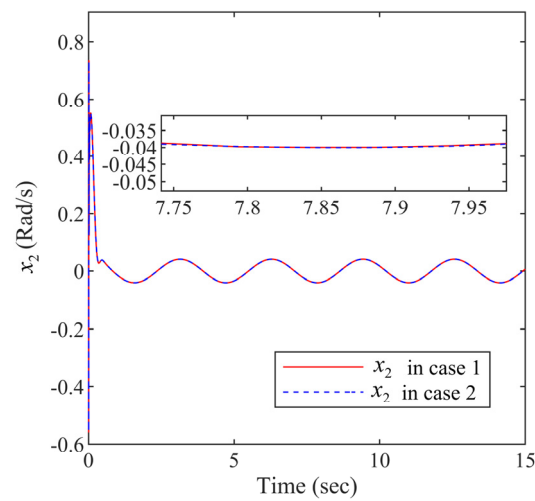


Figure 5. The state variable  $x_2$  responses.

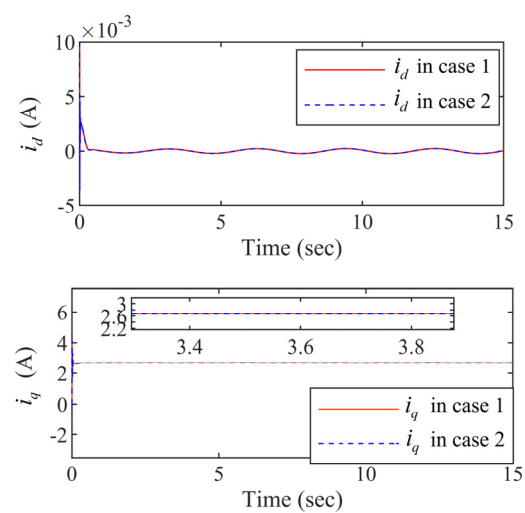
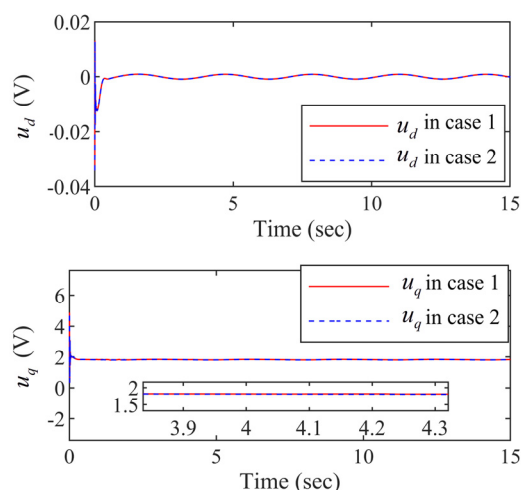


Figure 6. The state variables  $i_d$  and  $i_q$  responses.





**Figure 7.** The controllers  $u_d$  and  $u_q$  trajectories.

It can be seen from Figure 3 that the FDSC method ensures the best convergence of output signal  $x_1$  when compared with PID and NDSC methods no matter in Case 1 or Case 2. And the output signal  $x_1$  based on the FDSC method is limited with the funnel prescribed boundaries when the output signal  $x_1$  based on the NDSC method is out of the boundary. The curve of output signal  $x_1$  in case 1 is almost the same as it in case 2, which means that Lyapunov-Krasovskii functional can effectively address the time delays.

It is demonstrated from Figure 4 that the FDSC method has the smallest tracking error  $s_1$  among three control schemes no matter in Case 1 or Case 2. And the tracking error  $s_1$  based on the FDSC method is limited by the funnel prescribed boundaries when compared with the NDSC method. The curves of tracking error  $s_1$  are almost the same in the two cases, showing the effectiveness of the Lyapunov-Krasovskii functional.

It is shown from Figure 5 that the curve of the state variable  $x_2$  in Case 1 is almost the same as it in Case 2. It means that the Lyapunov-Krasovskii functional can effectively address the time delays. The controller designed in this paper guarantees that the state variable  $x_2$  in the closed-loop is controllable. The same conclusion can be drawn in Figure 6.

It can be seen from Figure 6 that the curves of the state variables  $i_d$  and  $i_q$  in case 1 are almost the same as them in case 2. It means that the Lyapunov-Krasovskii functionals can effectively address the time delays. The controller designed in this paper guarantees the stable operation of the PMSM systems with time delays. And the  $d$ -axis current  $i_d$  and the  $q$ -axis current  $i_q$  in the closed-loop are controllable. The same conclusion can be drawn in the Figure 7.

Within the funnel-type boundaries, Figure 3 gives the curves of output signal  $x_1$  and ideal signal  $x_d$  under three schemes (FDSC, PID, and NDSC). Figure 4 exhibits the curves of tracking error  $s_1$  for different scenarios. It can be concluded from Figures 3 and 4 that FDSC has a better convergency rate than NDSC, and the tracking error  $s_1$  of FDSC method is minimal compared to the other two options without breaking through funnel-type boundaries even considering the time delays. Figure 5 displays the curves of state  $x_2$  in the FDSC approach. Figure 6 illustrates the trajectories of states  $i_d$  and  $i_q$ , and Figure 7 shows the curves of controllers  $u_d$  and  $u_q$ . According to Figures 3–7, the states of the FDSC have extremely rapid response capability compared to NDSC and PID with time delays.

## 6. Conclusions

The FDSC with disturbance-observer has been investigated and suggested to resolve the position tracking control challenge for the PMSM with time delays here. At the beginning of this paper, an assumption and several lemmas are employed to uphold the control thesis and the design procedure of the funnel controller. With the aid of them, the inequalities in Section 3 can be simplified. Secondly, this paper introduces promising tools to eliminate the nonlinear uncertainties in PMSMs. For instance, this paper introduces

RBFNNs to estimate the unknown functions because they can approximate the unknown hard-to-calculated functions that are in a closed set at any precision. For the unknown mismatched and matched external disturbance, this paper utilizes a finite-time second-order DO. The finite-time DO can approximate the unknown interference with a finite time speed. To remove the limitations of the output variable, a funnel variable is designed in this paper without the demand for precise initial values of the state variable. This paper uses the first-order filters to filtrate the multiple derivatives of the virtual controllers so that the “explosion of complexity” can be addressed. The Lyapunov-Krasovskii functionals are devised in the controller design procedure of this paper to deal with time delays and guarantee the stable operation of the PMSMs. Thirdly, with the aid of RBFNNs, the finite-time DO, first-order filters, and the Lyapunov-Krasovskii functionals, the controller design procedure can be finished based on the backstepping method. Despite that the devised FDSC method can provide outstanding tracking performance shown in Figures 3–7 for the output-constrained PMSM, the finite-time response rates need to be further improved by combining it with finite-time stability theory. In further research later, we will further study how to improve the finite time convergence of tracking error based on the FDSC scheme. For PMSMs are widely applied in many significant fields, the neural adaptive FDSC scheme can be extended to vehicles, electric elevators, and machine tools.

**Author Contributions:** Conceptualization, M.L. and J.Z.; methodology, M.L.; software, F.W.; validation, T.Z., formal analysis, J.Z.; investigation, T.Z.; resources, S.L.; writing—original draft preparation, M.L.; writing—review and editing, M.L.; supervision, J.Z.; project administration, S.L.; funding acquisition, S.L. All authors have read and agreed to the published version of the manuscript.

**Funding:** This work was supported in part by the National Key technologies Research and Development Program of China under Grants No. 32020YFB1713300 and No. 2018AAA0101803, in part by the Natural Science Foundation of China No. 51635003 and No. 61863005, in part by the Guizhou Province Postgraduate Innovation Fund No. YJSKYJ(2021)030, in part by Guizhou Provincial Science and Technology Projects No. (ZK [2022] 142), in part by the Guizhou optoelectronic information and intelligent application International Joint Research Center No. Qiankehe platform talents No. 5802[2019], in part by the Foundation of Key Laboratory of Advanced Manufacturing Technology, Ministry of Education, Guizhou University No. GZUAMT2021KF [11], in part by the Science and Technology Incubation Planning Project of Guizhou University No. [2020]75.

**Conflicts of Interest:** The authors declare no conflict of interest.

## Nomenclature

### Acronyms

PMSM	Permanent magnetic synchronous motor
SVPWM	Space vector pulse width modulation
NN	Neural network
RBFNN	Radial basis function neural network
DO	Disturbance observer
PPF	Prescribed performance function
FDSC	Funnel dynamic surface control
NDSC	Neural dynamic surface control
PID	Proportion integral differential
IAE	Integration over the absolute value of the error
ITAE	Integration over time and the absolute value of the error
ISE	Integration over squared error

**Variables**

$x_i, i = 1, \dots, 4$	State variables
$\Delta E$	External disturbance term
$\Delta I_i(x(t - \tau_i)), i = 1, \dots, 4$	Time delay terms
$\varphi^* \in R^l$	Desired weight vector of RBFNN
$\hat{\varphi}$	Updated weight vector
$\psi(X)$	Estimation error
$v_i = [v_{i1}, \dots, v_{im}]^T$	Receptive field centers
$\beta_i, i = 1, \dots, 4$	Unknown variables
$u_{ic}, i = 2, 3$	The output of first-order filters
$u_i$	Virtual controllers, the input of first-order filters
$\phi_i, i = 2, 3$	First-order filter errors
$\eta_1$	Modified funnel variable
<b>Functions</b>	
$f_1(t)$	Positive funnel prescribed performance function
$F_k(\cdot)$	Gain function over time
$G(t)$	Scaling function
$\xi_{ij} > 0$	Smooth functions in Lyapunov–Krasovskii functional $V_T$
<b>Parameters</b>	
$l > 1$	Node numbers of RBFNN
$\chi_i$	Widths of the Gaussian functions

**References**

1. Sirimanna, S.; Thanatheepan, B.; Lee, D.; Agrawal, S.; Yu, Y.; Wang, Y.; Anderson, A.; Banerjee, A.; Haran, K. Comparison of electrified aircraft propulsion drive systems with different electric motor topologies. *J. Propul. Power* **2021**, *37*, 733–747. [[CrossRef](#)]
2. Foitzik, S.; Doppelbauer, M. Fault tolerant control of a three-phase PMSM by limiting the heat of an inter-turn fault. *IET Electr. Power Appl.* **2022**, *16*, 158–168. [[CrossRef](#)]
3. Qiu, Z.; Chen, Y.; Guan, Y.; Kang, Y. Vibration noise suppression algorithm of permanent magnet synchronous motor for new energy vehicles. *Int. J. Heavy Veh. Syst.* **2022**, *29*, 48–70. [[CrossRef](#)]
4. Hu, D.; Yang, L.; Yi, F.; Hu, L.; Yang, Q.; Zhou, J. Optimization of speed response of super-high-speed electric air compressor for hydrogen fuel cell vehicle considering the transient current. *Int. J. Hydrogen Energy* **2021**, *46*, 27183–27192. [[CrossRef](#)]
5. Zhang, J.; Wang, S.; Li, S.; Zhou, P. Adaptive neural dynamic surface control for the chaotic PMSM system with external disturbances and constrained output. *Recent Adv. Electr. Electron. Eng.* **2020**, *13*, 894–905.
6. Swaroop, D.; Hedrick, J.K.; Yip, P.P.; Gerdes, J.C. Dynamic surface control for a class of nonlinear systems. *IEEE Trans. Autom. Control* **2000**, *45*, 1893–1899. [[CrossRef](#)]
7. Lv, Z.; Ma, Y.; Liu, J.; Yu, J. Full-state constrained adaptive fuzzy finite-time dynamic surface control for pmsm drive systems. *Int. J. Fuzzy Syst.* **2021**, *23*, 804–815. [[CrossRef](#)]
8. Jiang, Y.; Xu, W.; Mu, C.; Zhu, J.; Dian, R. An improved third-order generalized integral flux observer for sensorless drive of PMSMs. *IEEE Trans. Ind. Electron.* **2019**, *66*, 9149–9160. [[CrossRef](#)]
9. Ke, D.; Wang, F.; He, L.; Li, Z. Predictive current control for PMSM systems using extended sliding mode observer with hurwitz-based power reaching law. *IEEE Trans. Power Electron.* **2021**, *36*, 7223–7232. [[CrossRef](#)]
10. Lian, C.; Xiao, F.; Liu, J.; Gao, S. Analysis and compensation of the rotor position offset error and time delay in field-oriented-controlled PMSM drives. *IET Power Electron.* **2020**, *13*, 1911–1918. [[CrossRef](#)]
11. Ali, N.; Rehman, A.U.; Alam, W.; Maqsood, H. Disturbance observer based robust sliding mode control of permanent magnet synchronous motor. *J. Electr. Eng. Technol.* **2019**, *14*, 2531–2538. [[CrossRef](#)]
12. Raj, F.V.A.; Kannan, V.K. Particle swarm optimized deep convolutional neural sugeno-takagi fuzzy PID controller in permanent magnet synchronous motor. *Int. J. Fuzzy Syst.* **2022**, *24*, 180–201. [[CrossRef](#)]
13. Liu, M.; Lu, B.; Li, Z.; Jiang, H.; Hu, C. Fixed-time synchronization control of delayed dynamical complex networks. *Entropy* **2021**, *23*, 1610. [[CrossRef](#)] [[PubMed](#)]
14. Xu, Y.; Li, S.; Zou, J. Integral sliding mode control based deadbeat predictive current control for PMSM drives with disturbance rejection. *IEEE Trans. Power Electron.* **2022**, *37*, 2845–2856. [[CrossRef](#)]
15. Li, R.; Zhu, Q.; Yang, J.; Narayan, P.; Yue, X. Disturbance-Observer-Based U-Control (DOBUC) for nonlinear dynamic systems. *Entropy* **2021**, *23*, 1625. [[CrossRef](#)]
16. Wang, Y.; Yu, H.; Liu, Y. Speed-current single-loop control with overcurrent protection for PMSM based on time-varying nonlinear disturbance observer. *IEEE Trans. Ind. Electron.* **2022**, *69*, 179–189. [[CrossRef](#)]
17. Cho, H.J.; Kwon, Y.C.; Sul, S.K. Time-optimal voltage vector transition scheme for six-step operation of PMSM. *IEEE Trans. Power Electron.* **2021**, *36*, 5724–5735. [[CrossRef](#)]
18. Dai, C.; Guo, T.; Yang, J.; Li, S. A disturbance observer-based current-constrained controller for speed regulation of PMSM systems subject to unmatched disturbances. *IEEE Trans. Ind. Electron.* **2021**, *68*, 767–775. [[CrossRef](#)]

19. Ge, Y.; Yang, L.; Ma, X. HGO and neural network based integral sliding mode control for PMSMs with uncertainty. *J. Power Electron.* **2020**, *20*, 1206–1221. [[CrossRef](#)]
20. Xu, M.; Huo, Z.; Li, S.; Jiang, L. Active steering PMSM speed control with wavelet neural network. *Int. J. Veh. Des.* **2020**, *82*, 64–74. [[CrossRef](#)]
21. Xu, B.; Zhang, L.; Ji, W. Improved non-singular fast terminal sliding mode control with disturbance observer for PMSM drives. *IEEE Trans. Transp. Electrification.* **2021**, *7*, 2753–2762. [[CrossRef](#)]
22. Hou, Q.; Ding, S.; Yu, X. Composite super-twisting sliding mode control design for PMSM speed regulation problem based on a novel disturbance observer. *IEEE Trans. Energy Convers.* **2021**, *36*, 2591–2599. [[CrossRef](#)]
23. Shao, X.; Si, H.; Zhang, W. Event-triggered neural intelligent control for uncertain nonlinear systems with specified-time guaranteed behaviors. *Neural Comput. Appl.* **2021**, *33*, 5771–5791. [[CrossRef](#)]
24. Zheng, Z.; Lau, G.-K.; Xie, L. Event-triggered control for a saturated nonlinear system with prescribed performance and finite-time convergence. *Int. J. Robust Nonlinear Control* **2018**, *28*, 5312–5325. [[CrossRef](#)]
25. Shi, Y.; Shao, X. Neural adaptive appointed-time control for flexible air-breathing hypersonic vehicles: An event-triggered case. *Neural Comput. Appl.* **2021**, *33*, 9545–9563. [[CrossRef](#)]
26. Zeng, Q.; Zhao, J. Event-triggered adaptive finite-time control for active suspension systems with prescribed performance. *IEEE Trans. Ind. Inf.* **2021**. [[CrossRef](#)]
27. Shao, X.; Si, H.; Zhang, W. Fuzzy wavelet neural control with improved prescribed performance for MEMS gyroscope subject to input quantization. *Fuzzy Sets Syst.* **2020**, *411*, 136–154. [[CrossRef](#)]
28. Wang, S.; Li, S.; Chen, Q.; Ren, X.; Yu, H. Funnel tracking control for nonlinear servo drive systems with unknown disturbances. *ISA Trans.* **2021**. [[CrossRef](#)]
29. Liu, C.; Wang, H.; Liu, X.; Zhou, Y. Adaptive finite-time fuzzy funnel control for nonaffine nonlinear systems. *IEEE Trans. Syst. Man Cybern. Syst.* **2021**, *51*, 2894–2903. [[CrossRef](#)]
30. Wang, S.; Ren, X.; Na, J.; Zeng, T. Extended-state-observer-based funnel control for nonlinear servomechanisms with prescribed tracking performance. *IEEE Trans. Autom. Sci. Eng.* **2017**, *14*, 98–108. [[CrossRef](#)]
31. Bao, J.; Wang, H.; Xiaoping Liu, P. Adaptive finite-time tracking control for robotic manipulators with funnel boundary. *Int. J. Adapt. Control Signal Process.* **2020**, *34*, 575–589. [[CrossRef](#)]
32. Zhu, Q.; Xiong, L.; Liu, H. A robust speed controller with smith predictor for a PMSM drive system with time delay. *Int. J. Control Autom. Syst.* **2017**, *15*, 2448–2454. [[CrossRef](#)]
33. Xing, H.; Ploeg, J.; Nijmeijer, H. Smith predictor compensating for vehicle actuator delays in cooperative ACC systems. *IEEE Trans. Veh. Technol.* **2019**, *68*, 1106–1115. [[CrossRef](#)]
34. Vadivel, R.; Joo, Y.H. Reliable fuzzy  $H_\infty$  control for permanent magnet synchronous motor against stochastic actuator faults. *IEEE Trans. Syst. Man Cybern. Syst.* **2021**, *51*, 2232–2245. [[CrossRef](#)]
35. Shanmugam, L.; Joo, Y.H. Design of interval type-2 fuzzy-based sampled-data controller for nonlinear systems using novel fuzzy Lyapunov functional and its application to PMSM. *IEEE Trans. Syst. Man Cybern. Syst.* **2021**, *51*, 542–551. [[CrossRef](#)]
36. Gong, C.; Hu, Y.; Gao, J.; Wang, Y.; Yan, L. An improved delay-suppressed sliding-mode observer for sensorless vector-controlled PMSM. *IEEE Trans. Ind. Electron.* **2020**, *67*, 5913–5923. [[CrossRef](#)]
37. Si, W.; Qi, L.; Hou, N.; Dong, X. Finite-time adaptive neural control for uncertain nonlinear time-delay systems with actuator delay and full-state constraints. *Int. J. Syst. Sci.* **2019**, *50*, 726–738. [[CrossRef](#)]
38. Wei, L.; Qian, C. Adaptive control of nonlinearly parameterized systems: The smooth feedback case. *IEEE Trans. Autom. Control* **2001**, *47*, 1249–1266.
39. Qian, C.; Wei, L. Non-Lipschitz continuous stabilizers for nonlinear systems with uncontrollable unstable linearization. *Syst. Control Lett.* **2015**, *42*, 185–200. [[CrossRef](#)]
40. Fang, W.; Bing, C.; Chong, L.; Jing, Z.; Meng, X. Adaptive neural network finite-time output feedback control of quantized nonlinear systems. *IEEE Trans. Cybern.* **2018**, *48*, 1839–1848.
41. Wang, H.; Sun, W.; Liu, P.X. Adaptive intelligent control of nonaffine nonlinear time-delay systems with dynamic uncertainties. *IEEE Trans. Syst. Man Cybern. Syst.* **2017**, *47*, 1474–1485. [[CrossRef](#)]
42. Yang, X.; Zheng, X. Adaptive nn backstepping control design for a 3-dof helicopter: Theory and experiments. *IEEE Trans. Ind. Electron.* **2020**, *67*, 3967–3979. [[CrossRef](#)]
43. Liu, H.; Pan, Y.; Cao, J.; Wang, H.; Zhou, Y. Adaptive neural network backstepping control of fractional-order nonlinear systems with actuator faults. *IEEE Trans. Neural Networks Learn. Syst.* **2020**, *31*, 5166–5177. [[CrossRef](#)]
44. Wang, H.; Li, M.; Zhang, C.; Shao, X. Event-based prescribed performance control for dynamic positioning vessels. *IEEE Trans. Circuits Syst. II Express Briefs* **2021**, *68*, 2548–2552. [[CrossRef](#)]
45. Li, F.; Liu, Y. Prescribed-performance control design for pure-feedback nonlinear systems with most severe uncertainties. *SIAM J. Control Optim.* **2018**, *56*, 517–537. [[CrossRef](#)]
46. Levant, A.; Livne, M. Globally convergent differentiators with variable gains. *Int. J. Control* **2018**, *91*, 1994–2008. [[CrossRef](#)]
47. Zhao, K.; Song, Y.; Zhang, Z. Tracking control of MIMO nonlinear systems under full state constraints: A single-parameter adaptation approach free from feasibility conditions. *Automatica* **2019**, *107*, 52–60. [[CrossRef](#)]
48. Yue, H.; Wei, Z.; Chen, Q.; Zhang, X. Dynamic surface control for a class of nonlinearly parameterized systems with input time delay using neural network. *J. Franklin Inst.* **2020**, *357*, 1961–1986. [[CrossRef](#)]